



Effects of Optical feedback in polymer-based tunable lasers

Master's Thesis of

Tianwen Qian

at the Karlsruhe School of Optics & Photonics
in cooperation with Fraunhofer Heinrich-Hertz-Institut

Reviewer: Prof. Dr. rer. nat. Uli Lemmer

Second reviewer:

Advisor: David de Felipe Mesquida

July 2018 – December 2018

Karlsruhe Institute of Technology
Karlsruhe School of Optics & Photonics
Schlossplatz 19
76131 Karlsruhe | Germany

I herewith declare that the present thesis is original work written by me alone, that I have indicated completely and precisely all aids used as well as all citations, whether changed or unchanged, of other theses and publications, and that I have observed the KIT Statutes for Upholding Good Scientific Practice, as amended.

Karlsruhe, 15.12.2018

.....

(Tianwen Qian)

Abstract

Integrated tunable lasers have been broadly used in DWDM coherent coommunication systems, where narrow linewidth is important in order to use high-order phase-sensitive modulation formats, and in access or passive optical networks (PON), where large direct modulation bandwidth and small chirp are crucial. In this Master's thesis, the effects of using feedback in order to reduce linewidth, increase modulation bandwidth and reduce chirp in DBR tunable lasers based on hybrid photonic integration on polymer are studied. Measurements for such laser under feedback show different behavior in lasing spectrum and improvement in linewidth, bandwidth and chirp. Additionally, photonic integrated circuits (PICs) where an on-chip feedback circuit has been implemented in order to control the optical-feedback effect and use it in a beneficial way, are presented. Photon-photon resonance is first achieved in polymer-based tunable laser and opens the door for future enhancement of the modulation bandwidth using this effect.

Contents

| | |
|--|----|
| Abstract | i |
| 1. Introduction | 1 |
| 2. Theory of External Optical Feedback in a Polymer-based DBR Laser | 3 |
| 2.1. Model of External Optical Feedback in a Polymer-based DBR Laser | 3 |
| 2.2. Chirp Reduction | 6 |
| 2.3. Linewidth Reduction | 6 |
| 2.4. Bandwidth Enhancement | 8 |
| 2.4.1. Detuned Loading Condition | 8 |
| 2.4.2. Feedback Introduced Detuned Loading | 9 |
| 2.4.3. Photon-Photon Resonance | 11 |
| 3. Tunable Laser with Feedback from the Output Waveguide Facet | 13 |
| 3.1. Effect of Feedback in the Lasing Spectrum | 13 |
| 3.2. Measurement of Feedback Effects on Linewidth | 17 |
| 3.3. Measurement of Feedback Effects on Bandwidth | 20 |
| 3.3.1. Detuend loading condition | 21 |
| 3.3.2. Feedback Introduced Detuned Loading | 21 |
| 3.4. Chirp Parameter (α -factor) Measurement | 23 |
| 3.4.1. Measurement with Lightwave Component Analyzer | 23 |
| 3.4.2. AM-FM Index Method | 25 |
| 4. Towards Tunable Laser with On-Chip Controllable Feedback | 27 |
| 4.1. Design and Characterization | 27 |
| 4.1.1. Short Feedback Cavity | 27 |
| 4.1.2. Long Feedback Cavity | 33 |
| 5. Conclusions & Outlook | 37 |
| Bibliography | 39 |
| A. Appendix | 43 |
| A.1. Detuned Loading Condition Calculation | 43 |
| A.2. Photon-Photon Resonance Calcuation | 44 |

1. Introduction

Increasing demand of high speed data transmission is affecting people's daily life and more advanced optical communication technology is needed to full this request, integrated tunable semiconductor laser is one of the important technologies.

The use of coherent communication in optical network systems is spreading rapidly to increase the transmission capacity [1], it is considered as a promising key technology to increase the spectral efficiency of optical transmission and to overcome the future capacity limitations of the currently installed fibre infrastructure [2]. Laser used in such systems requires narrow spectral linewidth because of the usage of the higher-order multi-level modulation format, such as 64QAM or beyond [2]. Single-frequency laser diodes such as Distributed Bragg Reflector (DBR) laser appears to be a good candidate for achieving narrow linewidth. Recently, linewidths of 350 kHz have been achieved [3], however, it is still limited by the short photon lifetime because of the relative short laser cavity. Concept of hybrid tunable lasers [4], which consists of an active section coupled to a passive waveguide section comprising tunable filters and reflectors, permits a narrower linewidth due to increased photon lifetime that is associated with an extended cavity length [5].

Besides, the directly modulated laser is a simple and reliable source for high speed optical communication. It is especially useful in short to medium distance applications (e.g. local area networks [6] and optical interconnects [7]) where the excess pulse dispersion due to laser chirp is not a critical issue [8]. It represents a relevant element to fulfill the continuously increasing need for low-cost optical communications systems with high bit-rate such as Fiber-To-The-Home (FTTH) [9, 10] and Passive Optical Network (PON) [11, 12] technology. In order to achieve large bandwidth and small chirp in directly modulated laser, using optical feedback effect by coupling the solitary laser with an ultra-short external cavity is reported as a possible solution [13, 14, 15].

The focus of this thesis is the study of the optical feedback effects on hybrid polymer-based tunable DBR laser and explore its possibility to decrease linewidth for coherent communication systems, improve bandwidth and reduce chirp for directly modulated laser. The tunable laser is constructed by a hybrid approach, combining polymer-based photonic integrated circuits (PIC) using Polyboard technology [16] with active Indium Phosphide (InP) components, which is shown in Figure 1.1. Theory relates to the laser coupled with a passive cavity is presented in chapter 2. Measurement results for the feedback characterization are presented in chapter 3. Finally, PolyBoard-based photonic integrated circuits (PIC) produced based on this work are then characterized and discussed in chapter 4.

1. Introduction



Figure 1.1.: Illustration of a tubal three-section DBR laser constructed by combining polymer-based phase and grating section with an active Indium Phosphide (InP) based gain section. The cleaved facet at the output waveguide side may introduce feedback effects depending on the way it is characterized.

2. Theory of External Optical Feedback in a Polymer-based DBR Laser

In this chapter, the modelling of external feedback in the hybrid polymer-based DBR laser considered in this work, is presented. This model is set as a starting point to discuss the effects of optical feedback with regards to linewidth, modulation bandwidth and chirp.

2.1. Model of External Optical Feedback in a Polymer-based DBR Laser

The effect of the external feedback in semiconductor lasers is defined by parameters of feedback coefficient C , coupling coefficient κ_{ext} and chirp reduction factor F [17, 18]. They are extracted by a three-mirror laser model and its equivalent two-mirror Fabry-Perot cavity as shown in Figure 2.1 in order to correctly consider the feedback effect in the polymer-based tunable DBR laser.

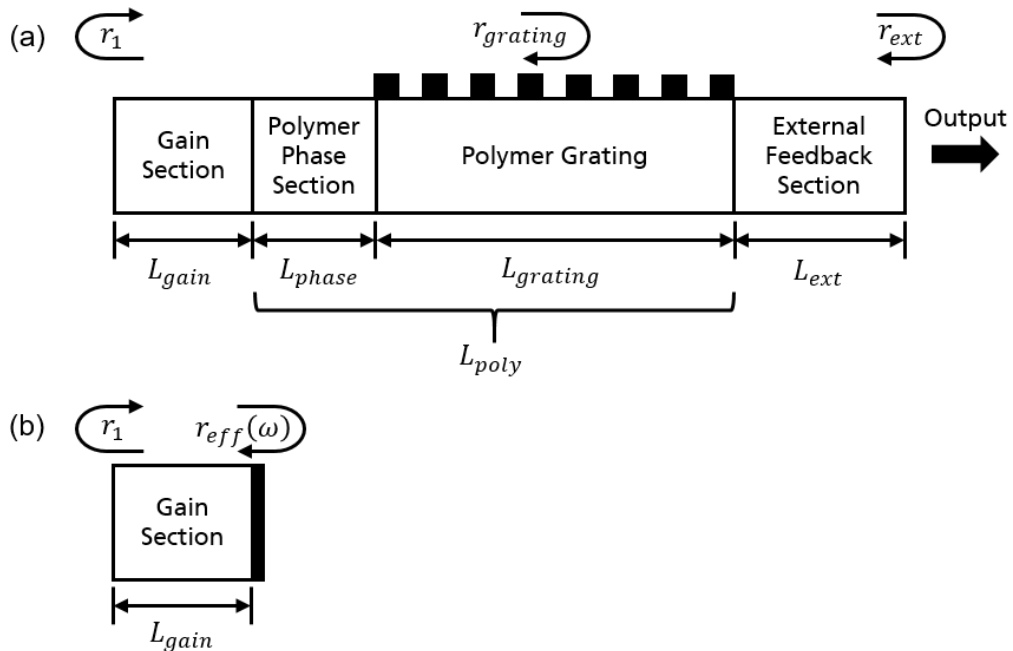


Figure 2.1.: (a) Polymer-based tunable DBR laser with external feedback section and (b) its equivalent cavity with effective mirror to model the feedback effect.

2. Theory of External Optical Feedback in a Polymer-based DBR Laser

The InP gain section in Figure 2.1 possesses a length of L_{gain} and comprises a High Reflection (HR) coating with reflectance r_1 at one of its facets and an Anti-Reflection (AR) coating against polymer at the other facet. The polymer part consists a phase and a grating section with a total length of L_{poly} and the external feedback section with a length of L_{ext} after the grating. r_1 , $r_{grating}$ and r_{ext} are amplitude reflectance of the gain section front facet, grating and external reflector respectively.

There are two ways to describe the feedback effect by the chirp reduction factor F , first one is mainly concerning the feedback coefficient C parameter, which characterizes the level of feedback in relation to how it affects the mode behavior of the laser and is defined as [18]

$$C = \frac{\tau_{ext}}{\tau_{gain} + \tau_{poly}} \kappa_{ext} \sqrt{1 + \alpha^2} \quad (2.1)$$

with

$$\kappa_{ext} = \frac{r_{ext}}{r_{grating}} \left(1 - |r_{grating}|^2 \right) \quad (2.2)$$

where $\tau = 2nL/c$ is the round-trip time in the corresponding section, κ_{ext} is the coupling coefficient from the grating reflector to the external cavity, and α is the linewidth enhancement factor [5]. Note that here the grating reflectivity $r_{grating}$ is considered as a constant value as shown in Figure 2.2, which leads to effective grating length $L_{eff} = \tanh(\kappa L_{grating})/2\kappa$ shorter than the real grating length $L_{grating}$ [19]. The L_{eff} is then contained in the laser cavity and the rest of the grating is included in the external feedback section.

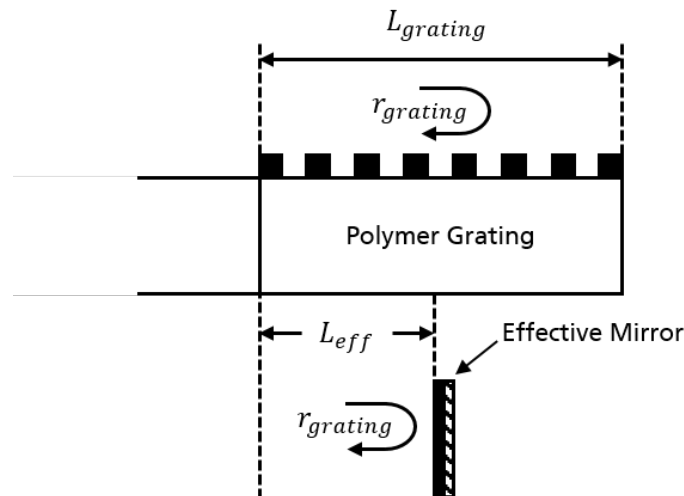


Figure 2.2.: Definition of an effective mirror for a grating reflector [20].

The C parameter indicates that the laser stability under feedback is affected both by external reflector r_{ext} and external round-trip time τ_{ext} . When $C < 1$, which implies weak feedback [18, 21], the laser operates in a single mode lasing region and is phase dependent to the external feedback [18, 21]. When $C > 1$, which implies medium to strong feedback [18, 21], over one stable mode will appear and the laser will undergo a route-to-chaos behavior until it reaches coherence-collapse [22] region. After the coherence-collapse region, if the feedback strength is even higher and the laser will operate in stable single mode again lasing with the compound cavity mode [23].

For the weak feedback region when $C < 1$, chirp reduction factor F is defined as [18, 20]

$$F = 1 + C \cos(\phi_{ext} + \arctan \alpha) \quad (2.3)$$

where $\phi_{ext} = 2\beta_{poly}L_{ext}$ is the round-trip phase of the external cavity.

For the case of strong feedback, which is more interesting and stable for the practical implementation, the factor F becomes [1]

$$F = 1 + R_{ext} \frac{\tau_{ext}}{\tau_{gain} + \tau_{poly}}. \quad (2.4)$$

where $R_{ext} = r_{ext}^2$ is the power reflectivity of the external reflector.

Second way to define the chirp reduction factor F is not only relate to round-trip time in each section but also to the frequency dependence of the reflection coefficient of the reflector [18]. In this work it is done by considering the equivalent two-mirror cavity and replacing the external feedback part with an effective mirror reflectivity $r_{eff}(\omega)$ as shown in Figure 2.1 (b), $r_{eff}(\omega)$ is modified according to [17, 20, 24]

$$r_{eff}(\omega) = r(\omega) \exp(-i\varphi_{eff}(\omega)) = \frac{r_{grating}(\omega) + r_{ext}W_1}{1 + r_{grating}(\omega)r_{ext}W_1} W_2 \quad (2.5)$$

$$W_1 = e^{-\alpha_{poly}L_{ext}} e^{-2i\beta_{poly}L_{ext}} \quad (2.6)$$

$$W_2 = e^{-\alpha_{poly}L_{phase}} e^{-2i\beta_{poly}L_{phase}} \quad (2.7)$$

where α_{poly} is the polymer waveguide propagation modal loss and $\beta_{poly} = 2\pi n_{poly}/\lambda$ is the effective propagation constant for the lasing mode, $r_{grating}(\omega)$ is the frequency-dependent complex amplitude reflectance of the grating reflector [25]. The chirp reduction factor F is then defined as [17, 18]

$$F = 1 + A + B \quad (2.8)$$

with

$$A = \frac{1}{\tau_{gain}} \left(\frac{d}{d\omega} \varphi_{eff}(\omega) \right) \quad (2.9)$$

$$B = \frac{\alpha}{\tau_{gain}} \left(\frac{d}{d\omega} \ln r_{eff}(\omega) \right) \quad (2.10)$$

where α is the linewidth enhancement factor [5], the parameter A is related to the frequency derivative of the phase $\varphi_{eff}(\omega)$ in Equation 2.5, which denotes the ratio of the external cavity path length to the gain section path length. It can be interpreted as the ratio of the photon numbers outside to inside the gain medium, which remains nearly constant once the laser cavity is formed [15]. By designing a cavity with a long external cavity, a large A can be achieved. On the other hand, the parameter B accounts for the wavelength dependence of the spectral reflectivity. It is changed if the lasing mode is detuned away from the Bragg wavelength under detuned loading conditions [26, 27, 28] which will be discussed further in Section 2.4. Additional reduction occurs only at the rising slope of the grating response which generates a positive B value.

2.2. Chirp Reduction

Light chirping can be defined as the instantaneous change of the central wavelength or optical frequency in response to variations in the optical power [29]. Two main contributions of the frequency chirp are distinguished, one is an adiabatic chirp, producing a frequency shift proportional to the instantaneous optical power, and is defined by parameter $\alpha_{adiabatic}$, which is associated to the nonlinear gain [29, 30]. Another one is a transient chirp component that evolves with the time derivative of the optical power, and is defined by $\alpha_{transient}$, normally named as linewidth enhancement factor [5] and dominates when dealing with semiconductor lasers [15].

The chirp reduction for laser coupled with a passive cavity is related to F and is defined as [15, 17, 18]

$$\alpha_{adiabatic} \approx \frac{\alpha}{1 + A + B} \quad (2.11)$$

$$\alpha_{transient} \approx \frac{\alpha(1 + A - B/\alpha^2)}{1 + A + B}. \quad (2.12)$$

Note that adiabatic chirp is usually frequency-independent and dominant at low modulation frequency, but for the semiconductor laser operating at large modulation frequency over 10 Gb/s, it is sufficient to consider only the transient chirp [15], which will be the one discussed in this thesis.

2.3. Linewidth Reduction

Linewidth reduction for laser coupled with a passive cavity is related to F and is defined as [17, 18]

$$\Delta\nu = \frac{\Delta\nu_0}{F^2} \quad (2.13)$$

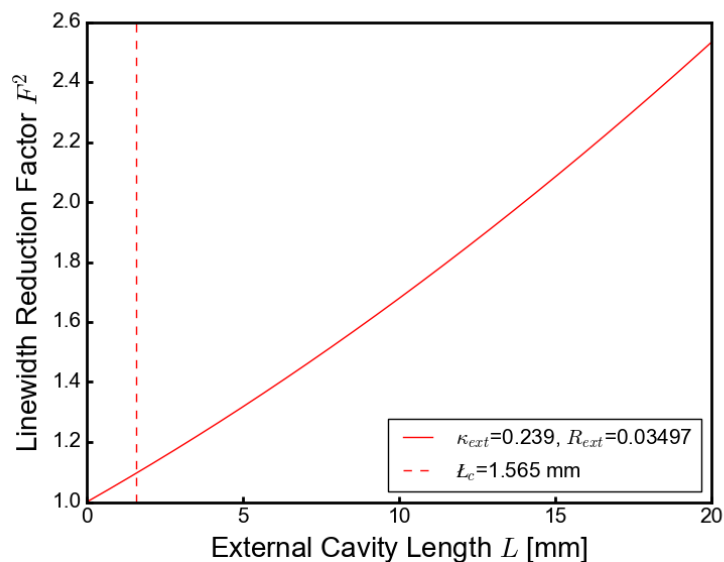
where $\Delta\nu$ and $\Delta\nu_0$ are the linewidth with and without feedback respectively.

For the weak feedback case, Equation 2.3 shows that the linewidth can either be narrowed $\Delta\nu_0/(1 + C)^2$ or broadened $\Delta\nu_0/(1 - C)^2$ depending on the feedback phase. Apart from that, Equation 2.8 shows further linewidth reduction can be achieved by considering the wavelength dependence of the spectral reflectivity introduced with parameter B .

With Equation 2.3 and Equation 2.4 the linewidth reduction factor F^2 versus the external cavity length can be calculated and is shown in Figure 2.3. Vertical dashed line L_c indicates more modes may start to appear where the C parameter reaches 1 [18]. Figure 2.3 is calculated under the assumption that the feedback comes from the output waveguide facet, which is formed by a polymer/air interface and leads to $R_{ext} = 0.035$. The parameters used for calculation is shown in Table 2.1.

Table 2.1.: Parameters used for the calculation of the linewidth reduction factor F^2 .

| Symbol | Description | Value |
|---------------|---------------------------------|----------------|
| L_{gain} | Active section length | $300 \mu m$ |
| L_{phase} | Phase section length | $525 \mu m$ |
| $L_{grating}$ | Grating section length | $699.84 \mu m$ |
| n_{gain} | Active section refractive index | 3.2 |
| n_{poly} | Polymer refractive index | 1.46 |
| α | Linewidth redcution factor | -3 |
| $R_{grating}$ | Grating reflectivity | 0.3 |
| R_{ext} | External cavity reflectivity | 0.035 |

Figure 2.3.: Calculated linewidth reduction factor F^2 assuming the feedback comes from the polymer/air interface. Dashed vertical line L_c indicates the length where the C parameter reaches 1 and more modes start to appear.

2.4. Bandwidth Enhancement

The maximum bit rate achieved by direct modulated lasers is typically limited by the well known resonance between carriers and photons, which is usually named as the carrier-photon resonance or the relaxation oscillation [20]. Three approaches to achieve broader bandwidth are explored in detail here.

2.4.1. Detuned Loading Condition

The first mechanism used to extend the modulation bandwidth of a semiconductor laser is the detuned loading effect, which is due to the frequency dependence of the reflection coefficient introduced by a distributed mirror (e.g. DBR [26, 27, 28]). It can be achieved without any external feedback.

The operation principle of the detuned loading condition can be illustrated by the calculated round-trip gain G curve, which is based on the effective laser cavity model presented in Section 2.1 and is defined as [18, 31]

$$G = r_1 e^{-2i\tilde{\beta}_{gain}L_{gain}} r_{eff}(\omega) = |G| e^{i\varphi(\omega)} \quad (2.14)$$

with [20]

$$\tilde{\beta}_{gain} = \beta + i\beta_i = \beta + \frac{i}{2}(g - \alpha_{in}) \quad (2.15)$$

where the real part $\beta = 2\pi n_{gain}/\lambda$ is the propagation constant inside the gain medium, and the imaginary part consists of the modal gain g and the internal modal loss α_{in} in the gain medium [20]. Cavity modes are obtained when round-trip gain in Equation 2.14 equals to 1 and the phase fulfills the integer values of $\varphi/2\pi$, e.g. for the lasing mode m at threshold one get [31]

$$|G(\lambda_m)| = G_m = 1, \varphi_m = 2m\pi \quad (2.16)$$

these two conditions allow to numerically find the lasing mode wavelength λ_m .

Parameters given in Table 2.2 were used to calculate the round-trip gain in a DBR laser cavity without feedback and the result is shown in Figure 2.4.

Table 2.2.: Parameters used for the calculation for the round-trip gain curve in a three-section DBR laser cavity.

| Symbol | Description | Value |
|---------------|---------------------------------|-----------------|
| L_{gain} | Active section length | $300 \mu m$ |
| L_{phase} | Phase section length | $525 \mu m$ |
| $L_{grating}$ | Grating section length | $700.644 \mu m$ |
| κ | Grating coupling coefficient | $9.80 cm^{-1}$ |
| n_{gain} | Active section refractive index | 3.2 |
| n_{poly} | Polymer refractive index | 1.46 |
| r_1 | Gain section reflectivity | 0.99 |

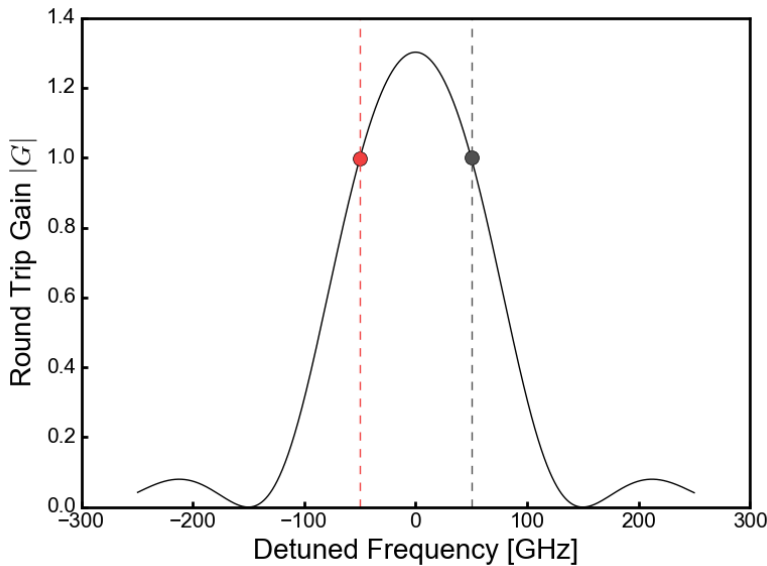


Figure 2.4.: Detuned loading condition with respect to the grating response. The red and grey markers correspond to the lasing mode detuend to the longer and shorter wavelength sides.

Detuned loading condition can be achieved by positioning the lasing mode at a slightly higher wavelength respect to the Bragg wavelength, as the red marker in Figure 2.4. It is reported that when the laser is operating at the longer wavelength side, an enhancement of modulation speed, reduction of phase noise (linewidth), and suppression of FM modulation (chirping) can be achieved [32].

The enhancement of the relaxation oscillation by detuned loading condition follows the same parameters A and B as defined in Equation 2.9 and Equation 2.10, which is given by [33]

$$\frac{f_r^2}{f_0^2} = \frac{1 + A + B}{(1 + A)^2 + (B/\alpha)^2} \quad (2.17)$$

$$\frac{\gamma_r}{\gamma_0^2} = \frac{1 + A}{(1 + A)^2 + (B/\alpha)^2} \quad (2.18)$$

where f_r and γ_r are the frequency and the damping rate of the relaxation oscillation, f_0 and γ_0 are the value for the solitary laser. As the parameter B indicates the slope of the grating response, by tuning towards the longer wavelength side, a positive B value can be achieved, thus an increase in the relaxation oscillation and lower damping value can be achieved according to Equation 2.17 and Equation 2.18.

2.4.2. Feedback Introduced Detuned Loading

Feedback introduced by a passive cavity can also contribute to the detuned loading effect [32, 34], it alters the frequency response of the effective reflector $r_{eff}(\omega)$ so that different A and B parmaerters can be utilised to further enhance the bandwidth. It has been reported that relaxation oscillation frequency f_r can be nearly doubled for external

2. Theory of External Optical Feedback in a Polymer-based DBR Laser

resonator lasers with an appropriate choice of the parameters A and B [32, 33, 34]. Feedback altered round-trip gain for such laser can be illustrated by using previously defined $r_{eff}(\omega)$ in Equation 2.5 and round-trip gain condition in Equation 2.16.

Parameters given in Table 2.3 were used to calculate the round-trip gain in a DBR laser cavity with external feedback coming from the output waveguide facet, which is formed by a polymer/air interface, the result is shown in Figure 2.5.

Table 2.3.: Parameters used for the calculation for the round-trip gain curve in a DBR laser cavity with feedback from a polymer/air interface.

| Symbol | Description | Value |
|---------------|----------------------------------|------------------|
| L_{gain} | Active section length | $300 \mu m$ |
| L_{phase} | Phase section length | $525 \mu m$ |
| $L_{grating}$ | Grating section length | $700.644 \mu m$ |
| L_{ext} | External feedback section length | $1473.363 \mu m$ |
| κ | Grating coupling coefficient | $9.80 cm^{-1}$ |
| n_{gain} | Active section refractive index | 3.2 |
| n_{poly} | Polymer refractive index | 1.46 |
| r_1 | Gain section reflectivity | 0.99 |
| r_{ext} | External reflector reflectivity | 0.187 |

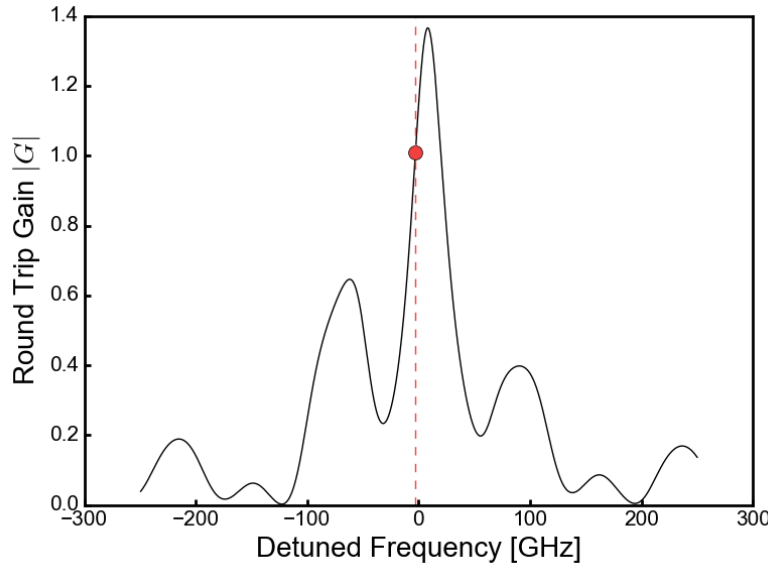


Figure 2.5.: Feedback introduced detuned loading condition with respect to the altered round-trip gain. The red marker corresponds to the lasing mode detuned to the longer wavelength side.

Compare to the round-trip gain without feedback shown in Figure 2.4, the detuning at the longer wavelength side shows a deeper slope which permits a larger B parameter, so that an further increase of relaxation oscillation can be achieved according to Equation 2.17.

2.4.3. Photon-Photon Resonance

Another approach used to extend the bandwidth takes advantage of the interaction between the lasing mode and an adjacent longitudinal cavity mode. If these two modes can be properly separated and interact due to the applied modulation signal at the gain section, it will introduce a resonance in the direct modulation response at the frequency corresponding to the mode separation [35]. This resonance is frequently called Photon-Photon resonance (PPR), to distinguish this interaction mechanism respect to the Carrier-Photon resonance (CPR) or Relaxation Oscillation (RO) [35]. The occurrence of the PPR should not be too far away from the relaxation oscillation frequency so that the dip between two peaks will not reach the -3 dB limitation in the modulation response as shown in Figure 2.6.

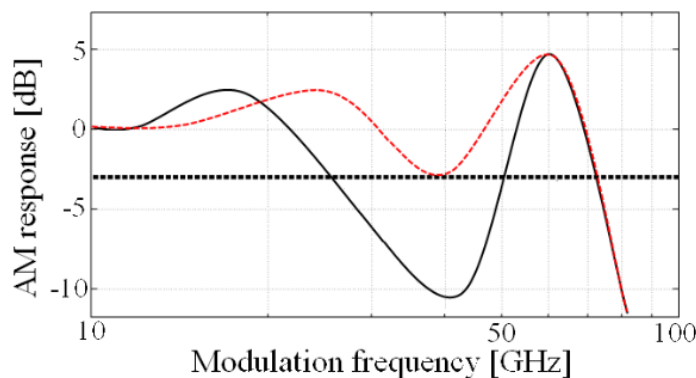


Figure 2.6.: Example of modulation responses obtained in a cavity exploiting the PPR effect. The black line indicates a case in which the CPR and the PPR peaks are too far whereas in the case indicated by the red line the modulation bandwidth extension is achieved [35].

The occurrence of the adjacent cavity mode has been observed to be closely related to the behavior of the cavity Round-Trip Phase (RTP) function [36], which refers to the phase factor $\varphi(\omega)$ in Equation 2.14. Calculation for a simplified DBR laser structure is done to illustrate the operation principle of the PPR. By assuming the DBR laser only contains a gain section and grating as in [35]. Parameters used for this calculation are shown in Table 2.4.

The calculated result is shown in Figure 2.7, where f_0 , f_1 and f_B denote the frequency of the lasing mode, PPR mode and the frequency corresponding to the Bragg wavelength. The most favorable operation condition is when the lasing mode at f_0 operates in the detuned loading condition $f_0 < f_B$, and a mode with frequency f_1 on the same side with respect to the Bragg wavelength is placed on the longer wavelength side of the Round Trip Gain (RTG) curve. In this mode configuration, the PPR effect can arise due to the coupling between the lasing mode and its adjacent mode [35], the corresponding PPR frequency is then the difference between these two modes. In order to generate an adjacent longitudinal cavity mode under feedback, a strong feedback condition is required [14, 37, 38, 39], which will form compound cavity modes with the Free Spectral Range (FSR) of the whole cavity considering the laser cavity plus the external feedback section as defined

2. Theory of External Optical Feedback in a Polymer-based DBR Laser

in Equation 2.19 [20]

$$\Delta\nu = \frac{c}{2(n_{gain}L_{gain} + n_{poly}(L_{phase} + L_{grating} + L_{ext}))} \quad (2.19)$$

this equation is also used as the design guideline in Section 4.1.

Table 2.4.: Parameters used for calculating the RTG and RTP for a simplified two-section DBR laser cavity without feedback [35].

| Symbol | Description | Value |
|-----------|------------------------------|--------------|
| L_A | Active region length | $140 \mu m$ |
| L_G | Grating region length | $780 \mu m$ |
| κ | Grating coupling coefficient | $20 cm^{-1}$ |
| n_{eff} | Effective refractive index | 3.7 |
| R_R | Right side reflectivity | 0 |
| R_L | Left side reflectivity | 0.32 |

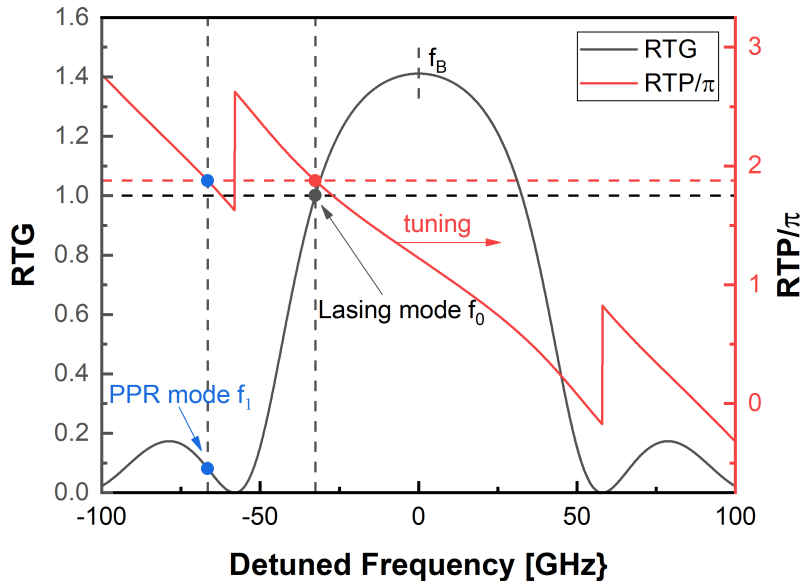


Figure 2.7.: Round trip gain (RTG, grey curve) and phase (RTP, red curve) functions calculated for a simplified two-section DBR laser without feedback. The grey and red marker represent the lasing mode at frequency f_0 on the corresponding RTG and RTP curve, the blue marker indicates the PPR mode at frequency f_1 .

3. Tunable Laser with Feedback from the Output Waveguide Facet

Characterization of the hybrid polymer-based tunable DBR laser linewidth, bandwidth and α parameter are measured with and without feedback from the output facet. This has been done by measuring with a cleaved fiber and using index-matching oil (case without optical feedback), and with a lensed fiber at the output and without index matching oil (case with feedback from the output waveguide facet), the two measurement configurations are shown in Figure 3.1. Principle of each measurement will be introduced and the results will be compared in the following sections.

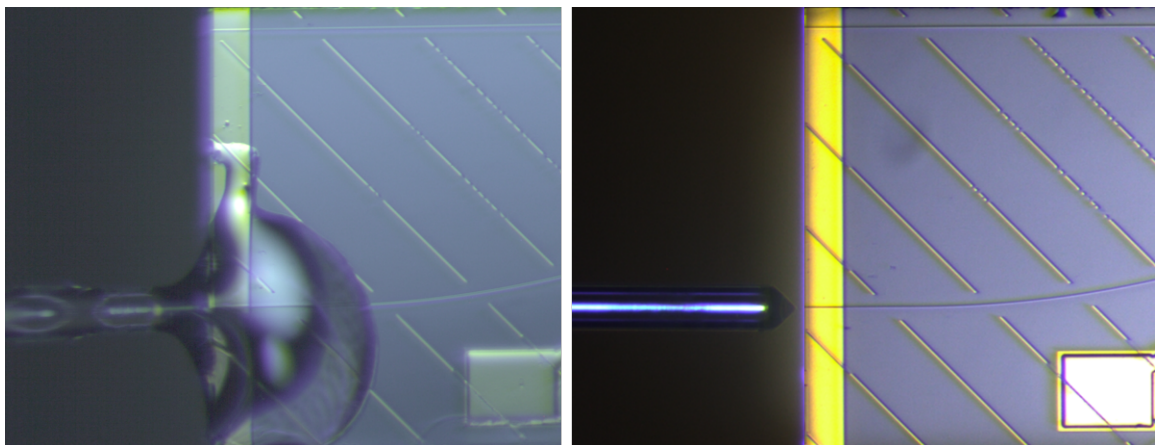


Figure 3.1.: (a) Measuring with cleaved fiber and using index-matching oil (case without optical feedback), (b) measuring with lensed fiber at the output and without index matching oil (case with feedback from the output waveguide facet).

3.1. Effect of Feedback in the Lasing Spectrum

With the effect of feedback, modes formed in the external feedback section between the grating reflector and the external reflector appear along with the modes in the laser cavity, they have different mode spacing because of their different section length, which is given by [20]

$$\Delta\nu_{cavity} = \frac{c}{2(n_{gain}L_{gain} + n_{poly}L_{poly})} \quad (3.1)$$

$$\Delta\nu_{ext} = \frac{c}{2n_{poly}L_{ext}} \quad (3.2)$$

3. Tunable Laser with Feedback from the Output Waveguide Facet

where L_{poly} and L_{ext} follow the definition in Section 2.1.

The spacing between the laser cavity mode and the mode formed in the external feedback section will change by tuning the phase through the increasing current, which in turn shifts the laser cavity modes towards the shorter wavelength side. The mode have the lowest cavity loss (highest intensiy) overalping with the grating response will become the lasing mode. The principle of wavelength tuning is presented in Figure 3.2.

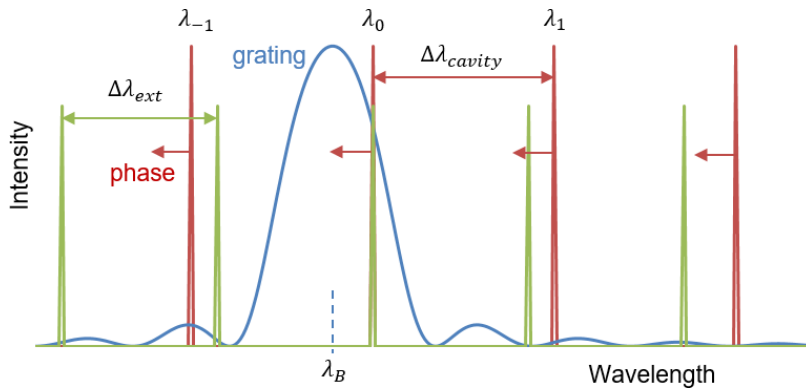


Figure 3.2.: Principle of phase tuning in tunable DBR laser. Red and green curves represent the mode of the laser cavity and external feedback section respectively, and the blue curve is the grating response.

The red and green curves in Figure 3.2 represent the laser cavity mode and the mode in the external feedback section, and the blue curve is the grating response. The different intensity considers that the feedback power is less than the output power. λ_0 is the lasing mode, λ_{-1} and λ_1 are its adjacent modes. λ_B is the Bragg wavelength which indicates the center of the grating response. $\Delta\lambda_{cavity}$ and $\Delta\lambda_{ext}$ are the mode spacing of the laser cavity and the external feedback section. The red arrow indicates the phase shifts the cavity modes toward the shorter wavelength through the increasing phase current. Besides the lasing mode, the interaction between the laser cavity mode and the mode formed in the external cavity is expected to appear at the grating side bands which will alter the lasing spectrum.

Examining the lasing spectrum for laser with feedback was done by measuring the central wavelength and Side-Mode-Suppression-Ratio (SMSR) simultaneously and then compared with the same measurement for laser without feedback. The measurements were done by fixing the gain section current at $I_{gain} = 80 \text{ mA}$, grating section current at $I_{grating} = 15 \text{ mA}$ and scanning the phase section from 4.5 mA to 30 mA with the step of 0.5 mA , the results are shown in Figure 3.3 and examples of spectra are shown in Figure 3.4.

3.1. Effect of Feedback in the Lasing Spectrum

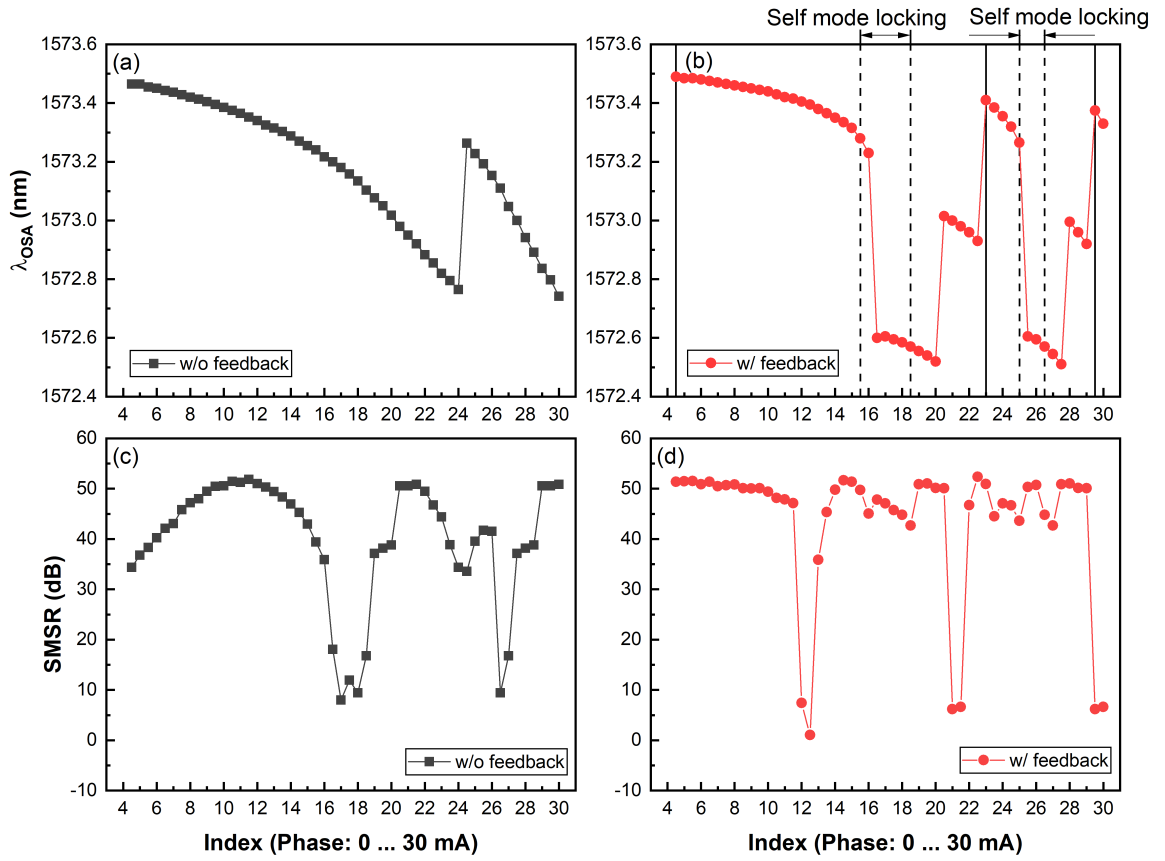


Figure 3.3.: Comparison of wavelength scanning (a), (b) and SMSR (c), (d) for tunable DBR laser with feedback (red circled curve) and without feedback (black squared curve).

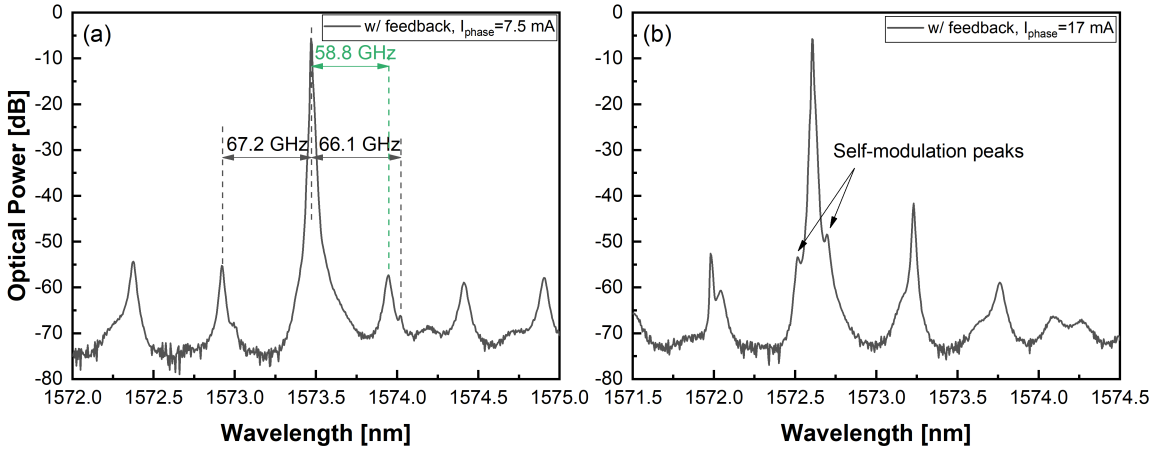


Figure 3.4.: Example of observed spectra for different phase current. (a) Green dashed line indicates the mode spacing between the main mode and the first side mode on the right, which corresponds to the laser cavity mode spacing $\Delta\nu_{\text{ext}} = 56.35 \text{ GHz}$, black dashed line indicates the mode spacing corresponds to the external feedback section $\Delta\nu_{\text{cavity}} = 67.04 \text{ GHz}$, (b) occurrence of the self-modulation peaks on both sides of the main mode are pointed with black arrows.

3. Tunable Laser with Feedback from the Output Waveguide Facet

Compare to the wavelength shifting behavior for laser without feedback in Figure 3.3 (a), additional hopping behavior in Figure 3.3 (b) appears due to the feedback effect. Using the parameters in Table 2.1 along with the external cavity formed between the end of the grating and the output waveguide facet with length of $L_{ext} = 1473.36 \mu m$, mode spacing for laser cavity and external feedback section were calculated as $\Delta\nu_{cavity} = 67.04 \text{ GHz}$ and $\Delta\nu_{ext} = 56.35 \text{ GHz}$ respectively. As seen from Figure 3.4 (a), the laser initially operates with the side mode spacing corresponds to the external feedback section, it is because with the feedback from the output waveguide facet $R_{ext} = 0.035$, the laser operates in the relative strong feedback region with $C = 1.69$ calculated by Equation 2.1. While shifting the phase current, small side peaks which relates to the behavior of self-modulation [40, 41] start to appear beside the main mode as shown in and Figure 3.4 (b).

Regarding to the cavity mode shifting principle, the occurrence of the self modulation peaks can be understood as a self mode locking behavior between the laser cavity mode and the mode in the external feedback section, which is reported in [42]. In this case, this term is used to name the region where these effects occurs, as shown in Figure 3.3 (b), to separate with the other lasing conditions along the phase shifting current.

Further understanding of the self-modulation peaks introduced by feedback was done by examining the lasing spectrum while tuning the wavelength through the phase current, the result is shown in Figure 3.11.

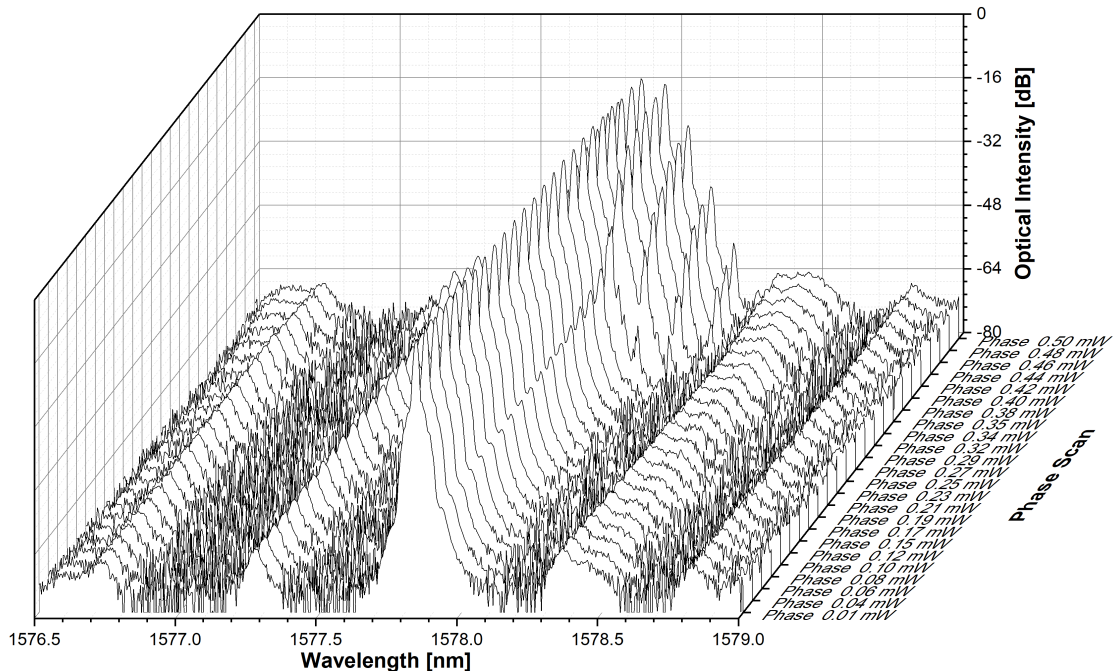


Figure 3.5.: Phase scan of the tunable DBR laser spectra with feedback from output waveguide facet. The side peaks of undamped RO start to appear, increase their intensity and shift toward the main peak. While the applied phase current keeps increasing, more peaks develop until the laser shift to another mode and operates as stable single mode lasing again.

Small satellite peaks in Figure 3.5 first show up with low phase current, then slowly increase their intensity and move towards the main peak, followed by more satellite peaks appearing which leads to the undamped relaxation oscillation [22, 43, 8] behavior where the mode spacing between the satellite peaks corresponds to the relaxation oscillation frequency [18].

The feedback introduced undamped relaxation oscillation behavior [22, 43, 8] can be understood as the incoming feedback acts like a perturbation for the laser cavity and introduces the amplitude modulation which is named as self-modulation [40, 41] or self-pulsation [18]. It can be explained that the increase of optical power from the feedback yields an increase of optical gain within the laser so that the round-trip gain reaches over one and optical power exponentially increases. On the other hand, an increased power yields an increasing consumption of carriers until the carrier density is too low to maintain a unity round trip gain and therefore the optical power collapses. A recovery time is required in order to increase the carrier density again until the next pulse develops. The repetition frequency for these pulses is of the same order as the relaxation resonance frequency [18].

3.2. Measurement of Feedback Effects on Linewidth

Feedback influenced laser linewidth is measured and compared with the laser linewidth without feedback condition. Self-homodyne method is used and the principle can be described mathematically as a single-delay autocorrelation, which is shown in Figure 3.6, the optical spectrum at f_0 autocorrelates with the delayed version of itself to produce a time-fluctuating spectrum, whose detected voltage has a power spectrum centered at zero frequency. For the case of a laser with Lorentzian lineshape, the half-width of the detected spectrum is equal to the linewidth of the laser.

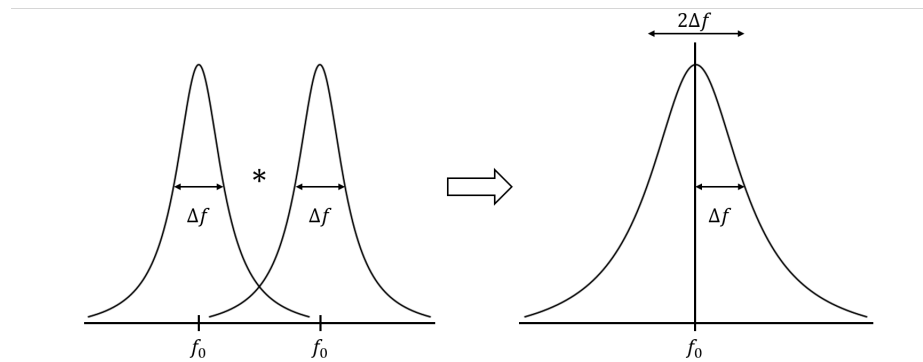


Figure 3.6.: Linewidth of a DBR laser using the self-homodyne technique. The optical spectrum at f_0 autocorrelates with the delayed version of itself to produce a time-fluctuating spectrum, whose detected voltage has a power spectrum centered at zero frequency, the half-width of the detected spectrum is equal to the linewidth of the laser.

The self-homodyne measurement set-up is shown in Figure 3.7. The input directional coupler of the interferometer splits the light from the laser into two paths. One path is delayed in order to decorrelate the combining signals, P_1 and P_2 . The output coupler

3. Tunable Laser with Feedback from the Output Waveguide Facet

combines the two signals, which are then mixed at the photodetector of the lightwave signal analyzer. The homodyne power spectrum is then observed on the analyzer from which the Lorentzian linewidth is measured by placing a marker at the half power frequency.

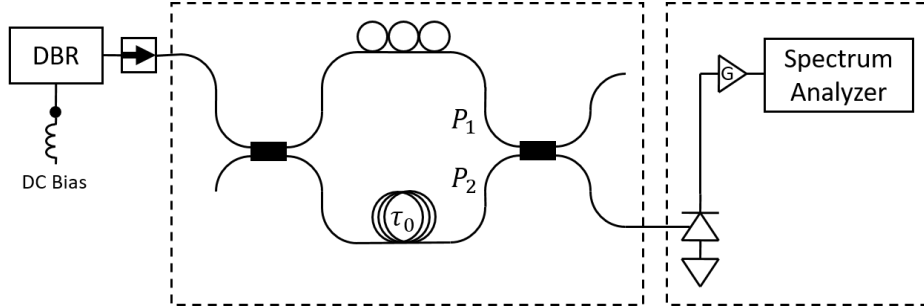


Figure 3.7.: Schematic set-up for self-homodyne linewidth measurement.

The results of linewidth measurement are shown in Figure 3.8. The laser linewidth under feedback shows a more stable transition and become narrower than the case without feedback. It is due to the reason that the external refelctor formed by the polymer/air interface with $R_{ext} = 0.035$ leads to $C = 1.69$, it is considered to be in the relative strong feedback region. In such case, the practical formula for linewidth reduction factor F^2 Equation 2.4 has to be considered. The comparison for the lowerest linewidth for two configurations, along with the theoretical predcition, is shown in Table 3.1.

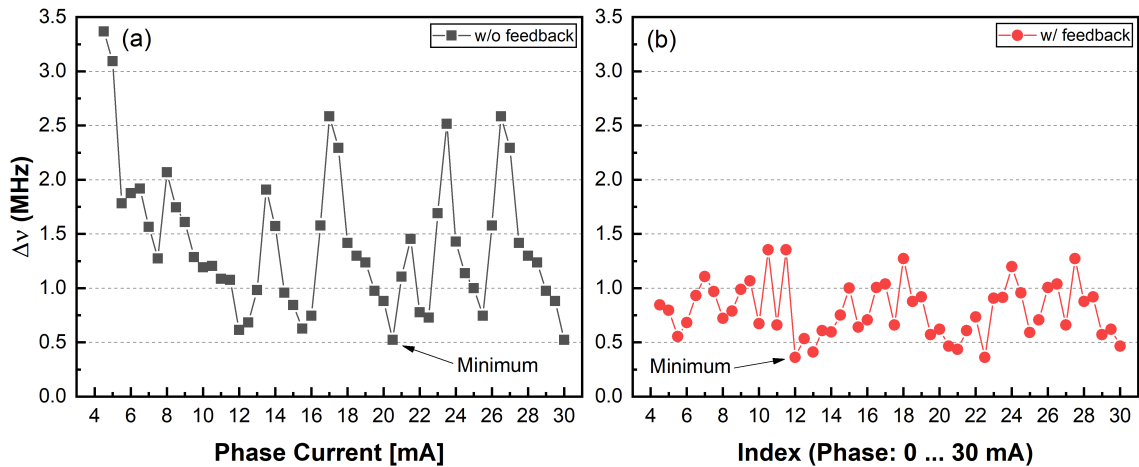


Figure 3.8.: (a) The laser linewidth without feedback from the output waveguide facet (b) laser linewidth with feedback from the output waveguide facet, it appears to be more stable compare to the laser without feedback. The achieved lowest linewidth point are pointed with black arrow in each case.

The difference between the measured and predicated value may comes from the assumption considered in Equation 2.4, since it mainly considers the ratio between the length of external feedback section and the laser cavity, which is mainly denoted as A paramter in the defination of F factor in Equation 2.8. The contribution from the frequency dependence

Table 3.1.: Comparison between the linewidth reduction value achieved by laser w/ and w/o feedback and the predicated reduction value.

| | w/o feedback | w/ feedback | Linewidth reduction factor F^2 | |
|-------------------|-----------------|---------------|----------------------------------|------------|
| | | | Measured | Predicated |
| $\Delta\nu$ [MHz] | 0.522 @ 20.5 mA | 0.360 @ 12 mA | 1.45 | 1.11 |

of the reflectance parameter B is not included which may further increase the predicated linewidth reduction factor.

3.3. Measurement of Feedback Effects on Bandwidth

Bandwidth for laser with feedback is compared with the case without feedback by the measurement of small signal modulation. Detuned loading condition achieved in both cases are presented. Photon-photon resonance is not observed because the feedback is not strong enough to form compound cavity modes.

The frequency response of a laser transmitter under small signal modulation is found by the usual assumption of a harmonic current modulation superimposed on a constant bias above threshold [44]. The modulation bandwidth f_{3dB} is a measure of the maximum modulation ability in semiconductor lasers through the injection current. It is usually defined as the frequency at which the modulation response has dropped by 3 dB relative to its zero frequency value [21, 45]. The characteristics of the small signal modulation in a normal laser are mainly determined by the relaxation oscillation frequency f_r , which indicated by the position of the peak in the modulation response.

The comparison of bandwidth for the polymer-based tunable laser was characterized at different gain current value. It was done by scanning through the gain current from 40 mA to 100 mA with a step of 5 mA and is presented in Figure 3.9.

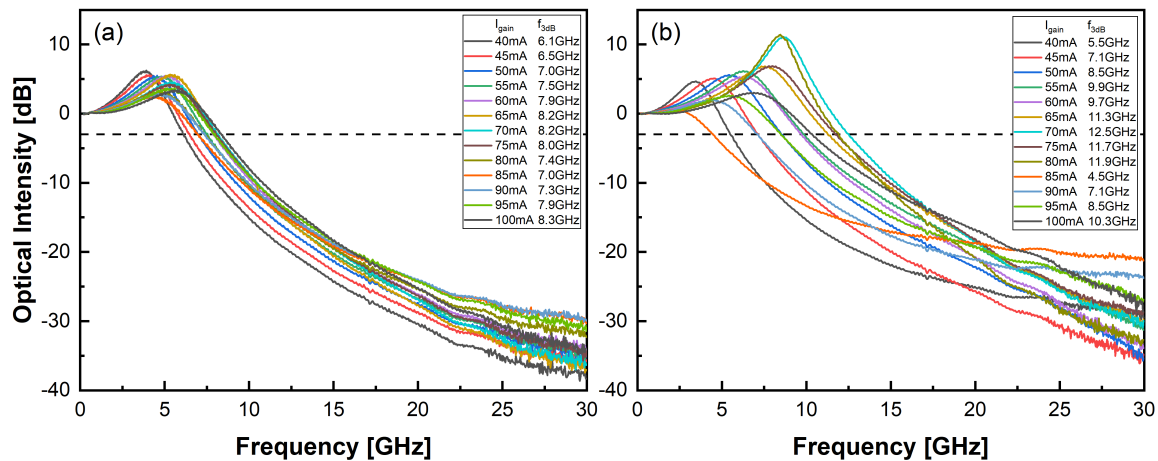


Figure 3.9.: Bandwidth measurements of a polymer-based tunable DBR laser. (a) Without feedback, the f_{3dB} shows a normal behavior that first increase with the applied gain current and then decrease, (b) with feedback, the prominent peaks at 65 mA and 70 mA permit the increased f_{3dB} value compare with the laser without feedback.

Without feedback, the increase of the relaxation oscillation frequency f_r along with rising of the gain current is observed and the intensity drop is due to the higher damping factor achieved at the higher gain current [18]. The maximum bandwidth achieved is 8.2 GHz at 65 mA and 70 mA.

Compare to Figure 3.9 (a), polymer-based tunable DBR laser operates differently with feedback, the intensity of the relaxation oscillation peak got enhanced especially at gain current I_{gain} between 65 mA and 80 mA, among these cases the maximum achieved bandwidth is 12.5 GHz at 70 mA. The reason will be further discussed in Subsection 3.3.2.

3.3.1. Detuned loading condition

In order to find the maximum achievable bandwidth for DBR laser without feedback, operating the tunable DBR laser under the detuned loading condition was measured and the result is shown in Figure 3.10. The measurement was performed by stabilizing the device at 25 °C and using a gain current $I_{gain} = 75 \text{ mA}$.

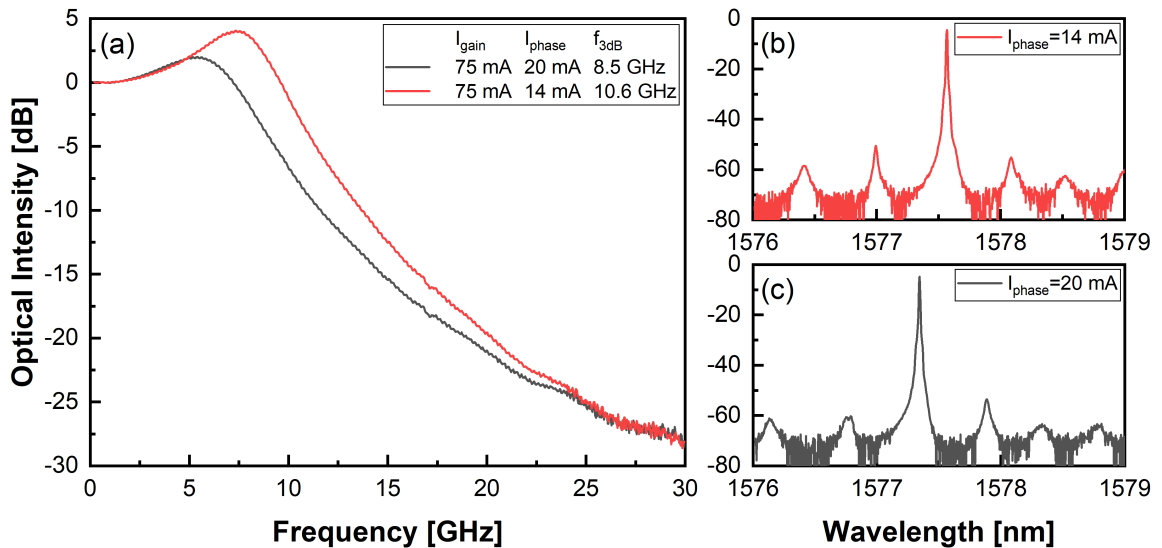


Figure 3.10.: (a) Bandwidth enhancement with the detuned loading condition on DBR tunable laser. The red curve is detuned to the longer wavelength side of the grating response and it shows an increased bandwidth of 2.1 GHz compared to the grey curve without bandwidth enhancement effect, (b) spectrum when laser operates at longer wavelength side, (c) spectrum when laser operates at lower wavelength side.

When the laser is lasing on the slope of the grating response, the side modes have a different gain spectrum relative to the peak of the grating response, which introduces the asymmetric behavior of the side modes as shown in Figure 3.10 (b) and (c). In this case, when the left side mode is higher than the right one, means the lasing mode is operating at the longer wavelength side of the grating response, and vice versa. By increasing the phase current I_{phase} from 14 mA to 20 mA, the lasing mode is detuned from the longer wavelength side of the grating response to the shorter wavelength side. The maximum f_{3dB} achieved at the longer wavelength side (red curve) is 10.6 GHz and the minimum (grey curve) is 8.5 GHz. These two operating points also corresponds to the red and grey points in Figure 2.4.

3.3.2. Feedback Introduced Detuned Loading

As discussed in Section 3.1, the feedback from the output waveguide facet acts like a perturbation for the polymer-based tunable DBR laser which leads to self-modulation and undamped RO while shifting the phase. Combining this spectral behavior with the dutuned loading condition under feedback, further investigation was done using the same setting as in Subsection 3.3.1, the result is shown in Figure 3.11.

3. Tunable Laser with Feedback from the Output Waveguide Facet

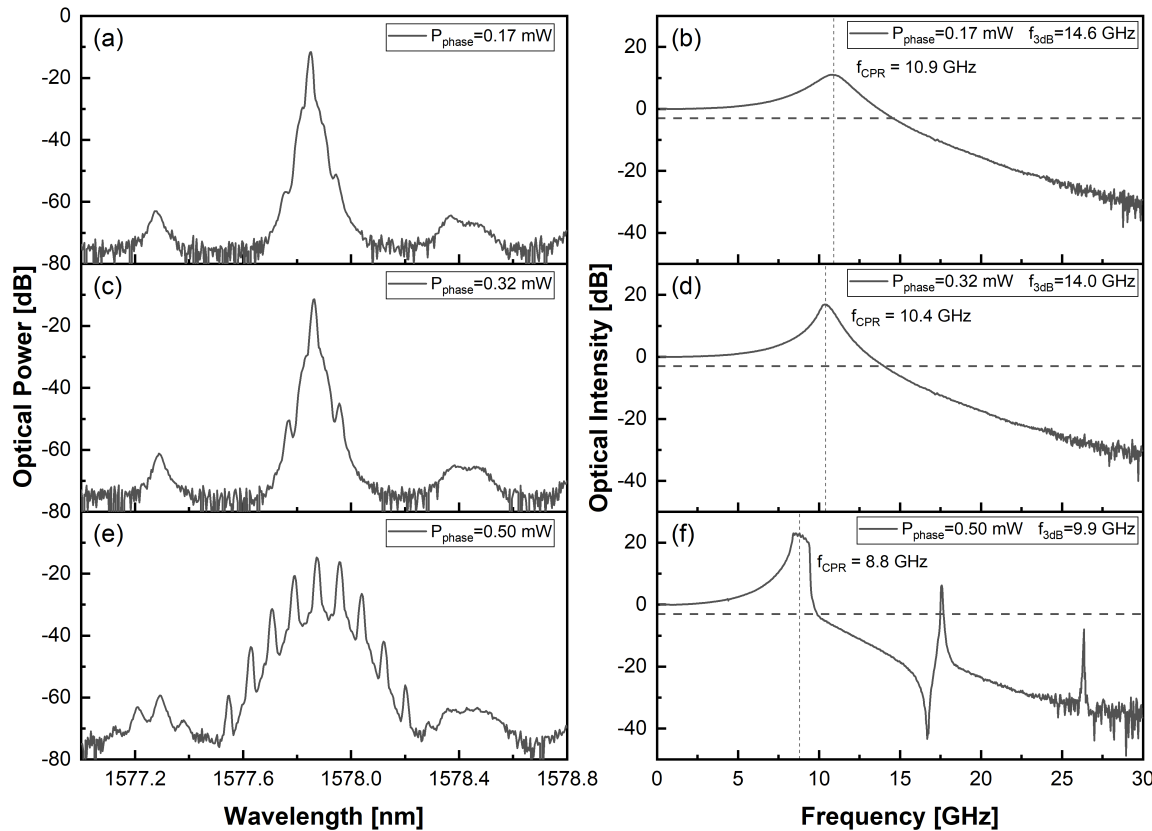


Figure 3.11.: Laser spectra and their corresponding intensity modulation curve. (a) Appearing of the undamped RO peak leads to a higher carrier-photon resonance in (b). (c) Growing of the side peaks leads to increase of the carrier-photon resonance peak in (d). (e) Drastic undamped RO leads to broadened lineshape and decreased modualiton bandwidth in (f).

The reason for the enhancement of the bandwidth can be seen from Figure 3.11. The appearing of the self-modulation side peaks leads to the carrier-photon resonance appears at a higher relaxation oscillation frequency which permits a higher f_{3dB} value of 14.6 GHz. Because of the phase tuning effect which relates to the dutuned loading condition, the side peaks slowly move towards the main peak with increasing intensity and the carrier-photon resonance become stronger with a slightly decreased relaxation oscillating frequency which leads to a f_{3dB} value of 14.0 GHz. As more side peaks appear in Figure 3.11 (e), the strong undamped RO behavior leads to a broader lineshape and the intensity modulation shows prominent peaks with frequency corresponding to the mode spacing of the lasing side peaks. This last behavior in Figure 3.11 (e) leads to broadened lineshape and significantly decreases the f_{3dB} compare to the other two cases. The increase of the relaxation oscillation intensity and the enhancement of bandwidth shown in Figure 3.9 (b) is certainly related to the occurence of the side peaks as shown in Figure 3.11 (a)-(d). The maximum achieved bandwidth f_{3dB} is 14.6 GHz for polymer-based tunable DBR laser with feedback. Photon-photon resonance was not observed in this case.

3.4. Chirp Parameter (α -factor) Measurement

Since the linewidth enhancement factor α is highly dependent on the spectral detuning [8], two measurement methods are performed to get the right characterization for DBR laser with feedback.

3.4.1. Measurement with Lightwave Component Analyzer

First method by using the Lightwave Component Analyzer (LCA) of Figure 3.12 measures the small signal frequency response of a light emitter, a dispersive medium and a light receiver. The dispersive medium is a standard single mode fiber of 81 km and an Er-doped fiber amplifier pumped at 1.55 μm . Resonance frequencies are observed as sharp peaks in the frequency response.

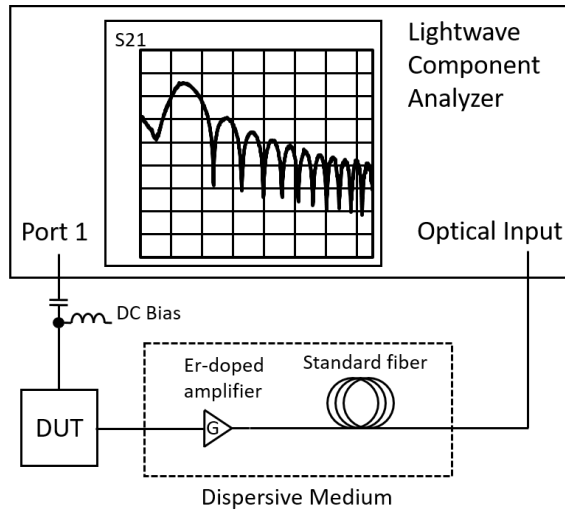


Figure 3.12.: Schematic set-up for chirp parameter measurement using Lightwave Component Analyzer.

The measurement principle can be explained as following, the output optical intensity is assumed as [46]

$$I = I_0(1 + m\cos(2\pi f t)) \quad \text{with } m \ll 1 \quad (3.3)$$

with m being the modulation depth and f the modulation frequency of light intensity. The frequency response which is measured by the set-up described above is then [46]

$$I_f = I_0 m \sqrt{1 + \alpha^2} \left| \cos \left(\frac{\pi \lambda^2 D L f^2}{c} + \arctan(\alpha) \right) \right|. \quad (3.4)$$

The resonance frequencies f_u (as shown in Figure 3.13 (a), (c)) correspond to the u^{th} -zeros of Equation 3.4. They follow the following equation [46]

$$f_u^2 L = \frac{c}{2D\lambda^2} \left(1 + 2u - \frac{2}{\pi} \arctan(\alpha) \right) \quad (3.5)$$

which is the result of two simultaneous interferences between the carrier and the two sidebands. Plotting $f_u^2 L$ versus $2u$ gives a straight line whose slope and position yield the dispersion and the chirp parameter by linear regression. The frequency of the first dip is determined primarily by α , and to a lesser extent by D , whereas the frequency of the second dip is determined primarily by D and to a lesser extent by α . D is the fiber dispersion coefficient [47].

The frequency response form LCA and fitted linear regression data are shown in Figure 3.13, the obtained α parameter in two conditions is compared in Table 3.2. The deviated α parameter at 80 mA with a value of 4.13 can be clearly seen from Figure 3.13 (c), whereas the position of the first dip of the purple curve which indicates 80 mA is deviated from the other current values, it may come from the effect of undmaped RO since in Figure 3.9 (b) at 80 mA the self-modulation introduced increase of relaxation oscillation peak appears. Except for this current value, the achieved α parmaeters with feedback are generally lower than the without feedback case. The different calculated F factor may come from shifting of the phase by increasing the current value.

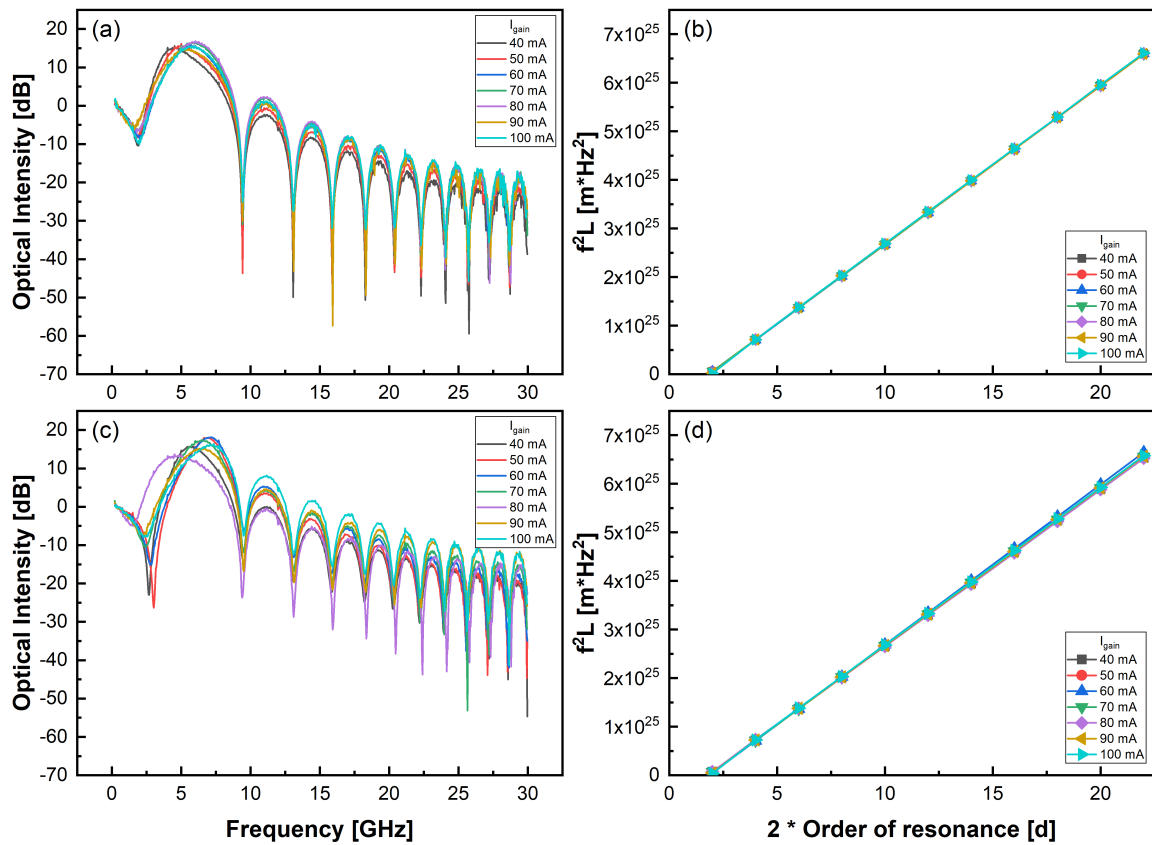


Figure 3.13.: Frequency response from the LCA measurement, (a) without feedback, (c) with feedback. Resonance frequencies squared (x-axis of (a) and (c)) times fiber length (81 km) versus two times the order of the resonance, (b) without feedback, (d) with feedback. Linear regression allows to find the chirp parameter and the dispersion from Equation 3.5.

Table 3.2.: Comparison of achieved α parameter value. Laser with feedback in general shows a decreased α value at all current values except for 80 mA. The different calculated F factor may come from shifting of the phase by increasing the current value.

| Current [mA] | α w/o feedback | α w/feedback | F Chirp reduction factor |
|--------------|--------------------------|------------------------|-------------------------------|
| 40 | 3.904 | 2.768 | 1.410 |
| 50 | 3.771 | 2.383 | 1.582 |
| 60 | 3.336 | 2.658 | 1.255 |
| 70 | 3.837 | 2.998 | 1.280 |
| 80 | 3.756 | 4.13 | 0.909 |
| 90 | 3.97 | 2.934 | 1.353 |
| 100 | 3.299 | 2.912 | 1.133 |

3.4.2. AM-FM Index Method

The α parameter can also be obtained from measurements of the optical intensity spectrum. For this measurement technique, the ratio of residual phase modulation to amplitude modulation is measured from the optical spectrum of the laser when it is modulated with a sinusoidal signal of frequency f , the output optical intensity is assumed same as Equation 3.3. The optical intensiy spectrum of this signal is characterized by an optical carrier with power I_0 , and two first oder sidebands with average power given by [30]

$$\overline{I_{\pm 1}} = I_0 \left(\frac{m}{4} \right)^2 \left(1 + \left(\frac{2p}{m} \right)^2 \right) \quad \text{with } m \ll 1 \quad (3.6)$$

where p is the phase modulation index [30], which is related to the chirp parameter by [48]

$$\frac{2p}{m} = \alpha \sqrt{1 + \left(\frac{f_c}{f} \right)^2} \quad (3.7)$$

where f_c is the chirp frequency. For modulation frequencies $f \gg f_c$, Equation 3.7 results to [30]

$$\frac{2p}{m} = \alpha \quad (3.8)$$

By measuring the power in the carrier and the sidebands from the optical spectrum, the paratmeter p can be obtained. The value of m can be obtained from the instantaneous power signal, therefore α parameter is characterized [29, 30].

The α parameter measurement results are shown in Figure 3.14. For laser with feedback the α parameter value ranges from -4.581 to -1.208 where as for laser without feedback it is from -4.944 to -2.36 . Lower α value of -1.208 is achieved for laser with feedback. It shows a similar result as the method in Subsection 3.4.1 and the α parameter under feedback conditions is decreased can be confirmed.

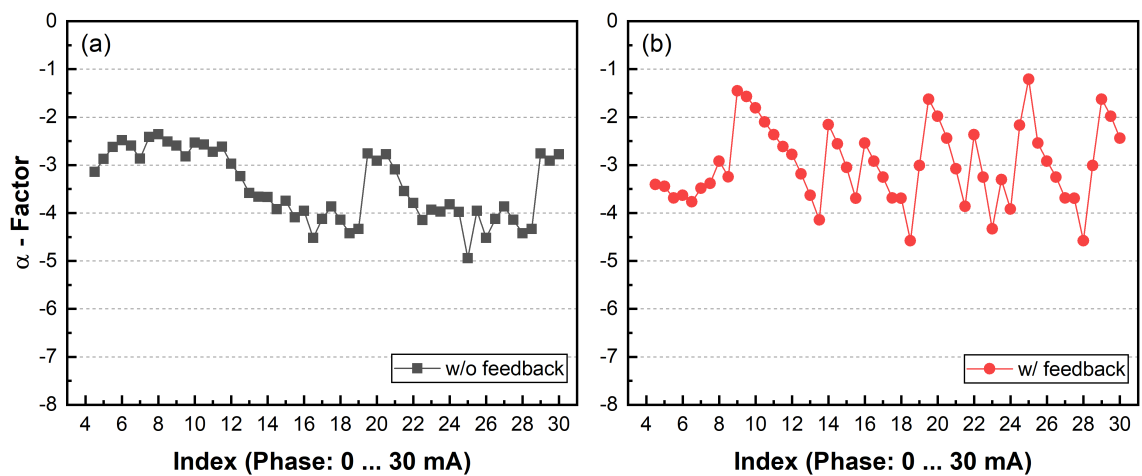


Figure 3.14.: (a) Measurement with cleaved fiber with oil, (b) measurement with lensed fiber, lower α parameter value is achieved.

4. Towards Tunable Laser with On-Chip Controllable Feedback

In this chapter, design of hybrid polymer-based tunable laser with on-chip controllable feedback is presented by combining the Polyboard technology [16] with InP components. Two separate designs are presented, one is focused on bandwidth enhancement by photon-photon resonance and the other is linewidth reduction. The elements used for the design and the first characterization of the produced photonic integrated circuits (PICs) are presented.

4.1. Design and Characterization

The design of the on-chip controllable feedback is targeting to the weak feedback region with phase dependent linewidth reduction and strong feedback region with compound cavity mode [18, 21]. Elements involved include the Bragg grating, Multimode Interferometer (MMI), Variable Optical Attenuator (VOA) and Thin Film Filter (TFF) structures on the Polyboard platform. Design principle and the characterization of the devices are shown in the following sections.

4.1.1. Short Feedback Cavity

The on-chip short feedback cavity design is shown in Figure 4.3, it is achieved by an additional waveguide and a TFF slot after the normal tunable DBR laser, followed by a 1×2 MMI to separate the output port and the external cavity. In the external cavity, VOA and phase section are included. The grating is designed to have its Bragg wavelength at $\lambda_B = 1550 \text{ nm}$. Variable Optical Attenuator (VOA) is achieved with a 1×1 thermally tunable MMI by placing an electrode on the side along the MMI which allows the thermo-optical effect. Thin Film Filter (TFF) acts as a high reflectivity mirror with its operating wavelength covers the grating Bragg wavelength, it can be simply inserted in the TFF slot thanks to the Polyboard technology.

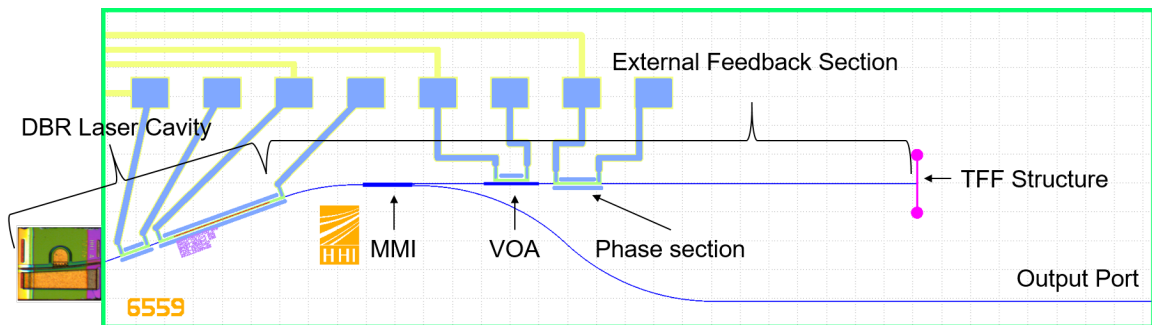


Figure 4.1.: Chip design of the laser with a short external section and controllable feedback.

In order to exploit PPR, Equation 2.19 is used to set the ideal cavity length in combine with Table 4.1 as shown below. External cavity length of [3129.76, 3589.76, 3859.76, 4159.76, 4869.76, 5309.76, 6359.76] μm are choosen according to the calculated FSR plot shown in Figure 4.2.

Table 4.1.: Parameters used for the calculation for PPR in the short feedback design.

| Symbol | Description | Value |
|---------------|---------------------------------|-------------|
| L_{gain} | Active section length | $300 \mu m$ |
| L_{phase} | Phase section length | $525 \mu m$ |
| $L_{grating}$ | Grating section length | $700 \mu m$ |
| n_{gain} | Active section refractive index | 3.2 |
| n_{poly} | Polymer refractive index | 1.46 |

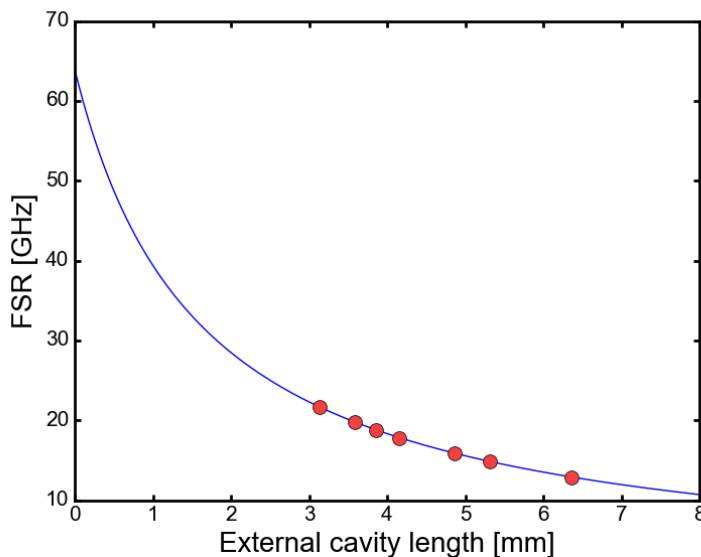


Figure 4.2.: FSR versus different external cavity length, the red circle markers are corresponding to the FSR of [21.7, 19.8, 18.8, 17.8, 15.9, 14.9, 12.9] GHz.

The example of produced photonic integrated circuits (PICs) and grating characterization is shown in Figure 4.3. The appearing of the ripples in the transmission and reflection curves indicates the existing of the strong reflection along with the grating. The calculated mode spacing is corresponding to the external feedback section and the distance between the MMI and the output port respectively, which indicates the reflection from the TFF slot is relatively high in this case. The characterization example of the VOA is shown in Figure 4.4. Maximum -28.39 dB damping was achieved at current value of 54 mA .

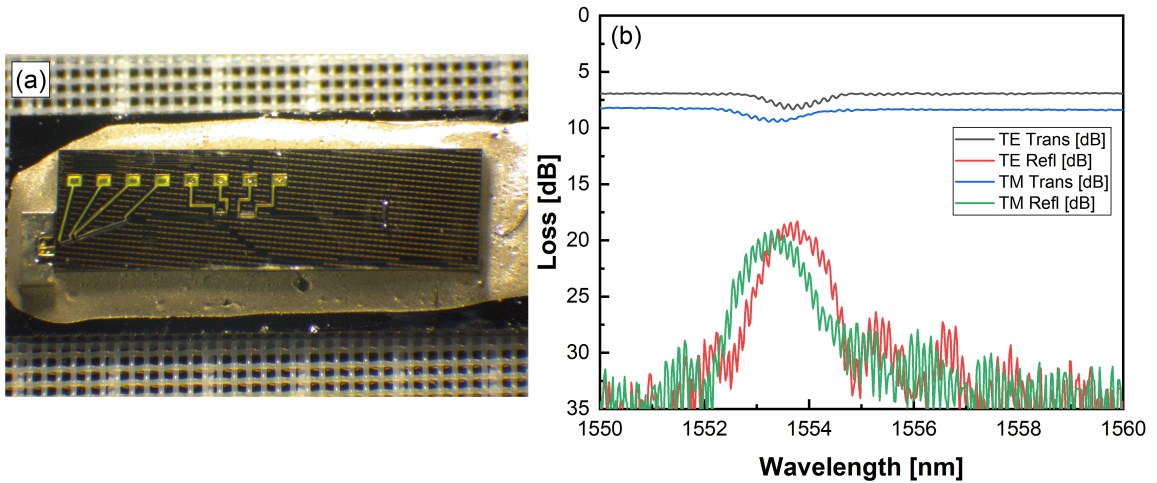


Figure 4.3.: (a) Produced photonic integrated circuits (PICs) with short feedback design, (b)grating characterization of the device, the spacing of the ripples in the transmission (black and blue) and reflection (red and green) curves are corresponding to the length of the external cavity and the distance between MMI and output port respectively.

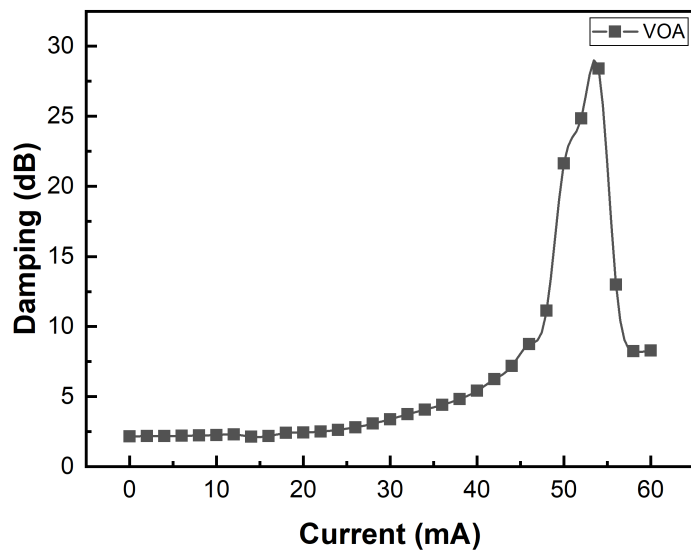


Figure 4.4.: Characterization of the VOA with maximum -28.39 dB damping achieved at current value of 54 mA .

4.1.1.1. Observed Photon-Photon Resonance

Bandwidth enhancement by PPR is achieved with this short external feedback design. As shown in Figure 4.5, the appearing of the second resonance peak in the frequency response is clearly different from the ones presented in Figure 3.11. The mode spacing of 15.2 GHz is corresponding to the external feedback section design of $4869.76\text{ }\mu\text{m}$ with FSR of 15.9 GHz , the appearing of PPR with value of 14.8 GHz is slightly lower than the FSR value but in the same order. By tuning the phase section in the external feedback section, the side mode shifts to the main mode and the PPR mode also moves toward the first peak which is CPR. Further tuning the phase section with the mode spacing close to the self mode locking range, the undamped RO starts to dominate and finally breaks the stable lasing condition.

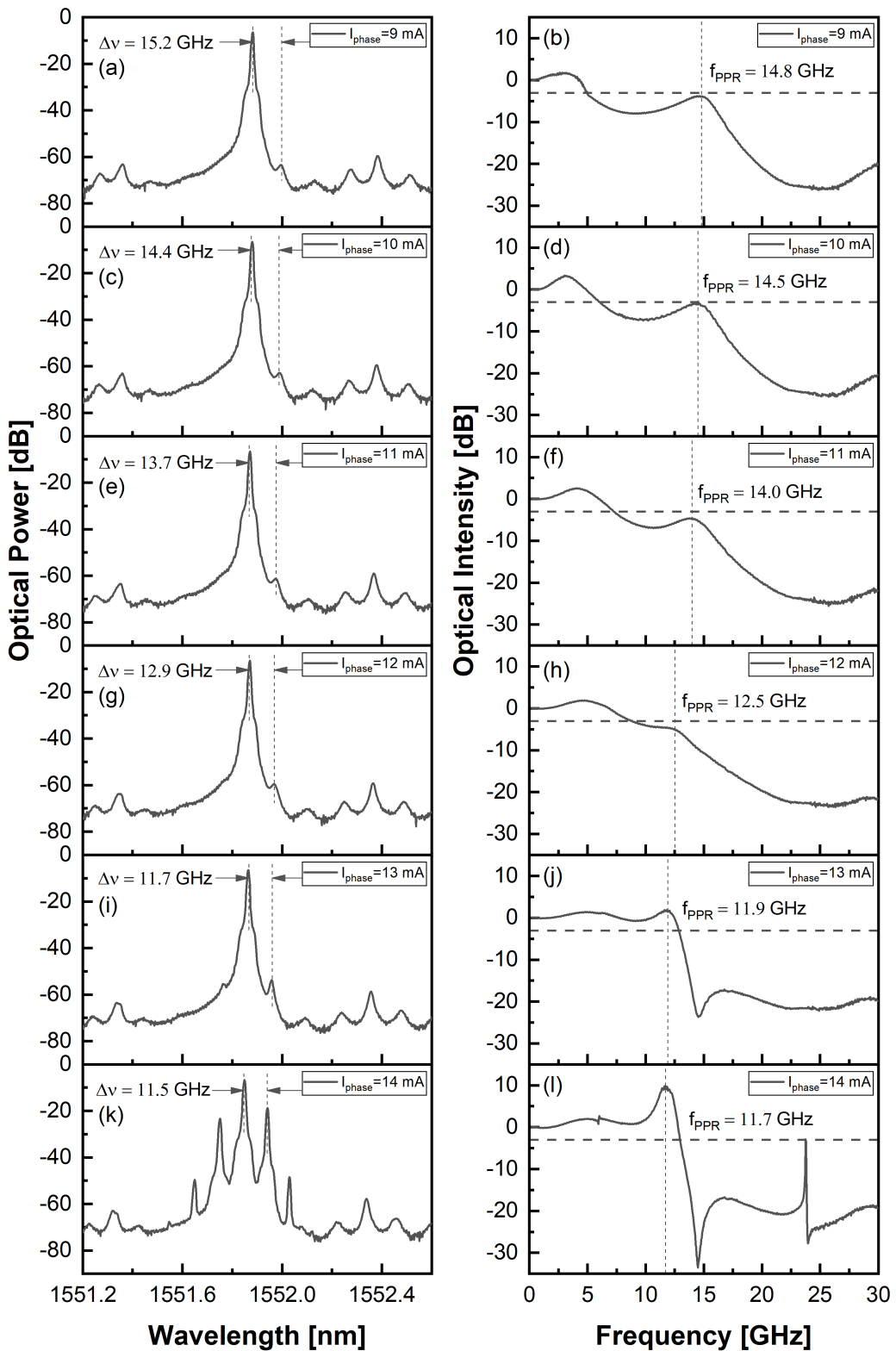


Figure 4.5.: Spectra and frequency response of the short external feedback device. Moving of the side peak in spectra and shifting of the second resonance peak in frequency response is observed by shifting the external feedback phase current.

The best achieved bandwidth value of $f_{3dB} = 13.2 \text{ GHz}$ with PPR is shown in Figure 4.6, with the external cavity length of $6359.76 \mu\text{m}$ and the designed FSR of 12.9 GHz . The mode spacing between the main mode and the side mode is 11.5 GHz and the PPR is appearing at 11.6 GHz in the frequency response.

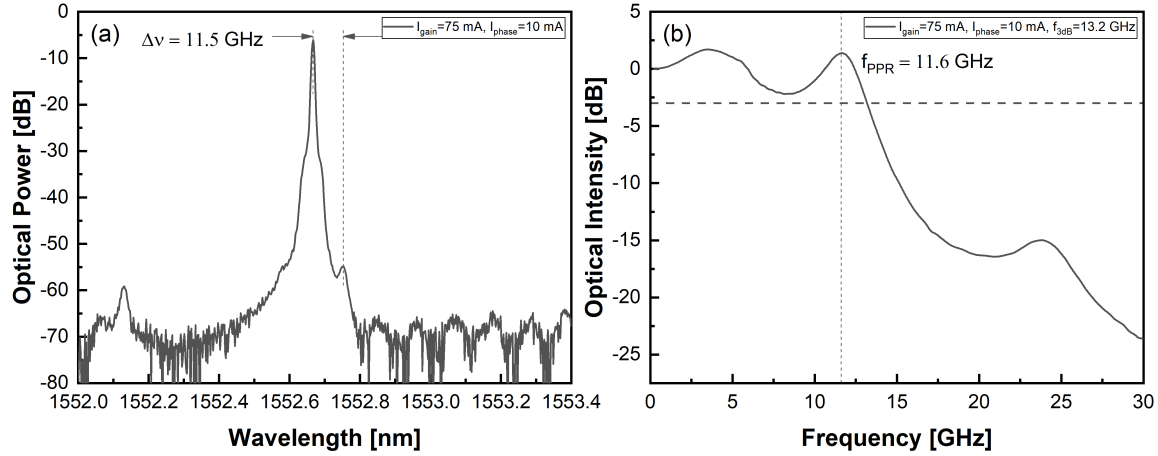


Figure 4.6.: The best achieved bandwidth value of $f_{3dB} = 13.2 \text{ GHz}$ with PPR. The external cavity length is $6359.76 \mu\text{m}$ corresponds to the FSR value of 12.9 GHz . The mode spacing between the main mode and the side mode is 11.5 GHz and the PPR is appearing at 11.6 GHz in the frequency response.

Chirp reduction is also observed by tuning the phase in the external feedback section, the result is shown in Figure 4.7 and Table 4.2. Tuning the phase current from 10 mA to 14 mA allows the increase of the α parameter from 1.793 to 3.245 . Note that the current value in Table 4.2 is 1 mA higher than the value in Figure 4.5 because of the existence of the hysteresis.

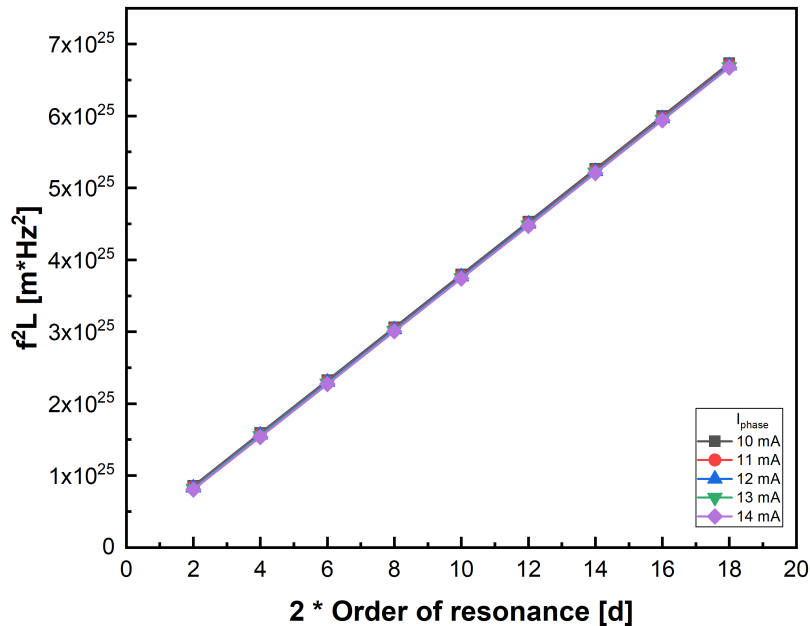


Figure 4.7.: Linear regression fit for phase current from 10 mA to 14 mA.

Table 4.2.: Measured chirp parameter α by fixing the gain current at 75 mA and scan the phase section in the external feedback section from 10 mA to 14 mA. Increasement of the chirp parameter α is observed from 1.793 to 3.245

| I_{gain} [mA] | α | | | | |
|-----------------|---------------------|---------------------|---------------------|---------------------|---------------------|
| | $I_{phase} = 10$ mA | $I_{phase} = 11$ mA | $I_{phase} = 12$ mA | $I_{phase} = 13$ mA | $I_{phase} = 14$ mA |
| 75 | 1.725 | 2.063 | 2.22 | 2.624 | 3.247 |
| 75 | 1.818 | 1.991 | 2.296 | 2.618 | 3.257 |
| 75 | 1.818 | 2.07 | 2.246 | 2.614 | 3.253 |
| 75 | 1.808 | 2.054 | 2.242 | 2.566 | 3.221 |
| Average | 1.793 | 2.045 | 2.251 | 2.606 | 3.245 |

The reason for the change of the α with respect to change of the phase current may relates to the slope of the feedback altered grating response as discussed in Subsection 2.4.2. By changing the phase current it shifts the lasing mode along the RTG curve towards the central peak which decreases the slope and in turn decreases the B parameter.

4.1.2. Long Feedback Cavity

Follows the same design principle as in Subsection 4.1.1, the long feedback section is achieved by the spiral structure with the circle bending radius of 1500 μm . The on-chip long feedback design is shown in Figure 4.8. The spiral structure has a variable design to achieve external cavity length of [39.28, 55.70, 81.33, 86.53, 100.75, 157.35] mm by using Equation 2.3 and Equation 2.4.

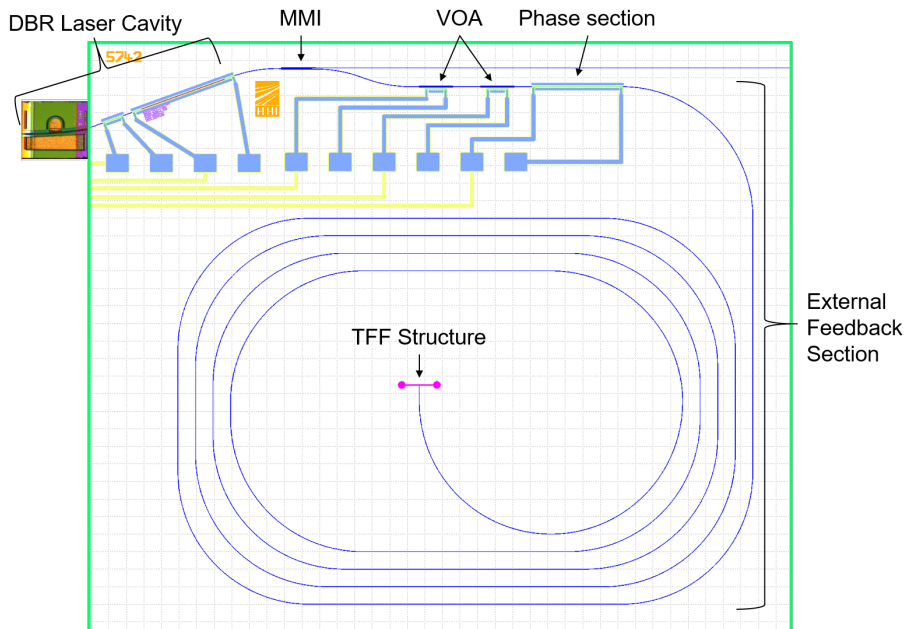


Figure 4.8.: Chip design of the laser with a long external section and controllable feedback.

The example of produced photonic integrated circuits (PICs) and grating characterization is shown in Figure 4.9. Similar ripples were observed in the reflection curves but not in the transmission curves, it may because the attenuation inside the polymer waveguide after the spiral structure is relative high so that the reflected from the TFF slot got attenuated.

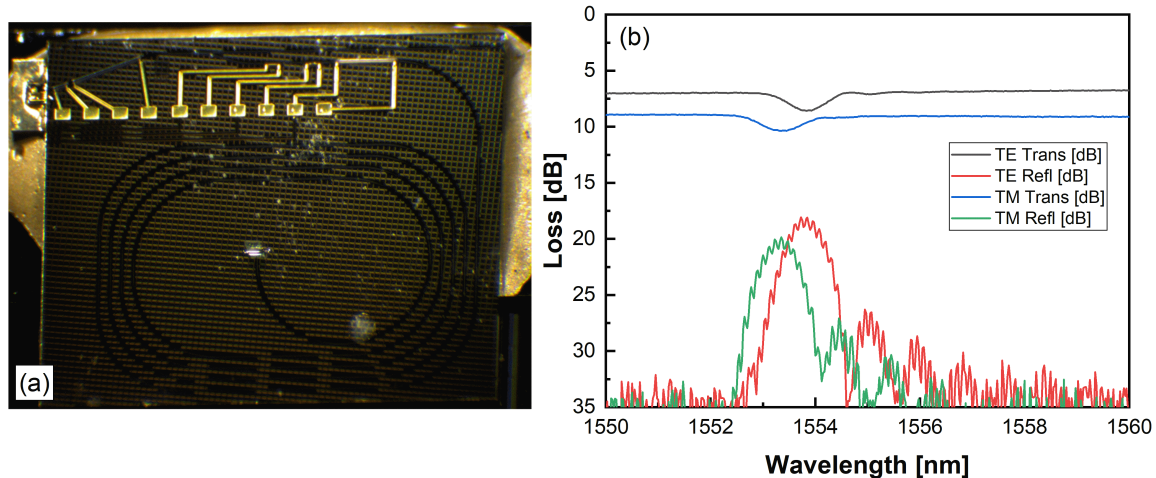


Figure 4.9.: (a) Produced photonic integrated circuits (PICs) with long feedback design, (b) grating characterization of the device, the spacing of the ripples in the reflection (red and green) curves are corresponding to the distance between MMI and output port.

Linewidth was measured using the same principle as in Section 3.2. External feedback phase current I_{ext_phase} was shifted from 14 mA to 30 mA with the step of 0.2 mA and the possible phase dependent linewidth reduction can be seen in Figure 4.10.

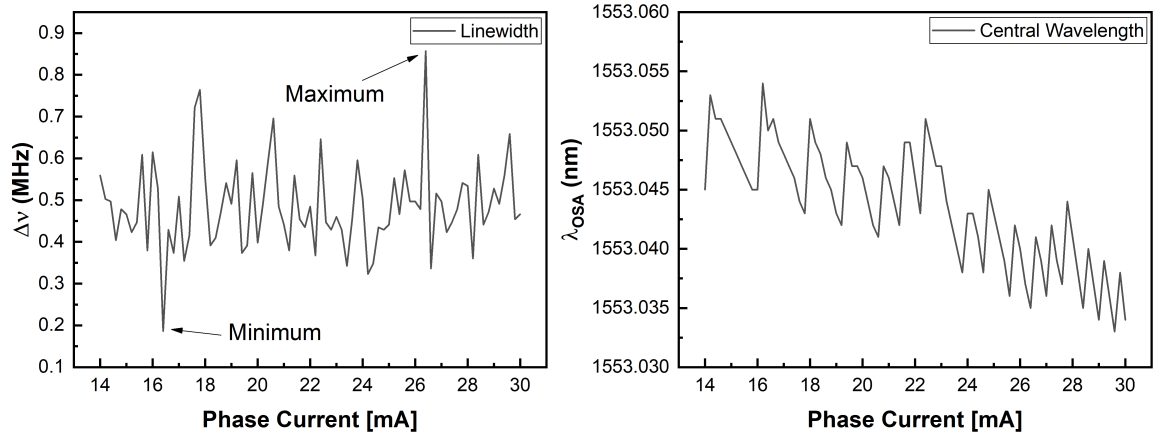


Figure 4.10.

Since from the grating characterization a possible high attenuation in the waveguide is observed, which leads to a assumption that this device is operating under relative weak feedback with parameter $C < 1$. From the wavelength scan a periodic shifting of the central wavelength indicates the feedback introduces a periodic effect to the laser cavity. With Equation 2.3, the periodic behavior was modeled with $\cos(\phi_{ext} + \arctan \alpha)$ term with the feedback round trip phase ϕ_{ext} included. More characterization needs to be done on such device since the minimum value achieved in Figure 4.10 is one isolated point in the scan of the phase, which could be not correctly calculated.

5. Conclusions & Outlook

Effect of feedback in polymer-based tunable DBR laser was investigated and compared with the case without feedback. The potential of linewidth reduction, bandwidth enhancement and chirp reduction for such laser was demonstrated.

Theory about feedback influenced laser cavity was modeled with the parameter F which affects the laser linewidth and chirp, the modelling was adapted to the type of tunable laser used in this work. Numerical calculation showed significant difference compared to the laser without feedback, which is possible for achieving better linewidth and bandwidth for polymer-based tunable laser. Measurements showed a linewidth reduction factor F^2 of 1.45 was achieved which led to laser linewidth of 360 kHz with optical feedback, the corresponding chirp reduction by F was also confirmed.

Feedback introduced spectra behavior such as self-modulation and undamped relaxation oscillation were observed in this work, the mechanism was studied by phase tuning measurements in combination with the detuned loading condition to explore the potential of extending the modulation bandwidth for polymer-based tunable laser. Bandwidth value of 10.6 GHz was achieved for laser without feedback whereas maximum of 14.6 GHz was achieved when the laser is under feedback condition with self-modulation peaks appearing in the spectrum. The appearing of such self-modulation peaks in lasing spectra can be used as an indicator for setting the laser working in the extended bandwidth region.

Further improvement of linewidth and bandwidth for polymer-based tunable laser was explored by designing an on-chip controllable feedback laser combining the DBR laser structure with two types of feedback sections. First, short feedback section design successfully achieved the photon-photon resonance for the first time on poly-based tunable DBR laser. The appearing of the second peak in the frequency response permits the extended bandwidth value to 13.2 GHz in this work. Second, long feedback section with spiral structure was presented. However, significant linewidth reduction has not been observed yet by this design. The problem so far seems like the feedback is not strong enough in such spiral design. Whether it is because of the high attenuation inside such waveguide structure or some fabrication issue or by coincident choice of the characterized device need to be investigated in a next stage.

The next steps building on these laser concepts are first the improvement of the achieved photon-photon resonance because so far the bandwidth value it achieved is still lower than the feedback introduced self-modulation case. Then further experiments cover the devices with other parameters in order to fully characterize this design.

Bibliography

- [1] Hiroyuki Ishii et al. “Narrow linewidth tunable DFB laser array integrated with optical feedback planar lightwave circuit (PLC)”. In: *IEEE Journal of Selected Topics in Quantum Electronics* 23.6 (2017), pp. 1–7.
- [2] Matthias Seimetz. “Laser linewidth limitations for optical systems with high-order modulation employing feed forward digital carrier phase estimation”. In: *Optical Fiber communication/National Fiber Optic Engineers Conference, 2008. OFC/NFOEC 2008. Conference on.* IEEE. 2008, pp. 1–3.
- [3] D De Felipe et al. “Hybrid polymer/InP dual DBR laser for $1.5 \mu\text{m}$ continuous-wave terahertz systems”. In: *Terahertz, RF, Millimeter, and Submillimeter-Wave Technology and Applications IX*. Vol. 9747. International Society for Optics and Photonics. 2016, p. 974719.
- [4] Youwen Fan et al. “Spectral linewidth analysis of semiconductor hybrid lasers with feedback from an external waveguide resonator circuit”. In: *Optics express* 25.26 (2017), pp. 32767–32782.
- [5] Charles Henry. “Theory of the linewidth of semiconductor lasers”. In: *IEEE Journal of Quantum Electronics* 18.2 (1982), pp. 259–264.
- [6] Wenjia Zhang, Howard Wang, and Keren Bergman. “Next-generation optically-interconnected high-performance data centers”. In: *Journal of Lightwave Technology* 30.24 (2012), pp. 3836–3844.
- [7] Marc A Taubenblatt. “Optical interconnects for high-performance computing”. In: *Journal of Lightwave Technology* 30.4 (2012), pp. 448–457.
- [8] Miguel C Soriano et al. “Complex photonics: Dynamics and applications of delay-coupled semiconductors lasers”. In: *Reviews of Modern Physics* 85.1 (2013), p. 421.
- [9] Adolfo Cartaxo, José AP Morgado, and Daniel Fonseca. “A perspective on optical-wireless converged NG-FTTH networks using directly modulated lasers”. In: *Transparent Optical Networks (ICTON), 2011 13th International Conference on.* IEEE. 2011, pp. 1–4.
- [10] V Khanaa, Krishna Mohanta, and T Saravanan. “Performance analysis of FTTH using GEPON in direct and external modulation”. In: *Indian Journal of Science and Technology* 6.6 (2013), pp. 4848–4852.
- [11] Ryohei Urata et al. “High performance, low cost, colorless ONU for WDM-PON”. In: *National Fiber Optic Engineers Conference.* Optical Society of America. 2012, NTh3E–4.

Bibliography

- [12] Jun-ichi Kani. "Enabling technologies for future scalable and flexible WDM-PON and WDM/TDM-PON systems". In: *IEEE Journal of Selected Topics in Quantum Electronics* 16.5 (2010), pp. 1290–1297.
- [13] Moustafa Ahmed and Ahmed Bakry. "Modulation performance of semiconductor laser coupled with an ultra-short external cavity". In: *Optics Communications* 360 (2016), pp. 52–60.
- [14] Shigeru Mieda et al. "Ultra-Wide-Bandwidth Optically Controlled DFB Laser With External Cavity". In: *IEEE Journal of Quantum Electronics* 52.6 (2016), pp. 1–7.
- [15] Byung-Seok Choi et al. "Evaluation of chirp reduction in polymer-based tunable external-cavity lasers". In: *IEEE Journal of Quantum Electronics* 51.1 (2015), pp. 1–15.
- [16] Z Zhang et al. "Polymer-based photonic toolbox: passive components, hybrid integration and polarisation control". In: *IET optoelectronics* 5.5 (2011), pp. 226–232.
- [17] R Kazarinov and C Henry. "The relation of line narrowing and chirp reduction resulting from the coupling of a semiconductor laser to passive resonator". In: *IEEE Journal of quantum electronics* 23.9 (1987), pp. 1401–1409.
- [18] Klaus Petermann. *Laser diode modulation and noise*. Vol. 3. Springer Science & Business Media, 2012.
- [19] Mark Kuznetsov. "Theory of wavelength tuning in two-segment distributed feedback lasers". In: *IEEE journal of quantum electronics* 24.9 (1988), pp. 1837–1844.
- [20] Larry A Coldren, Scott W Corzine, and Milan L Mashanovitch. *Diode lasers and photonic integrated circuits*. Vol. 218. John Wiley & Sons, 2012.
- [21] Junji Ohtsubo. *Semiconductor lasers: stability, instability and chaos*. Vol. 111. Springer, 2012.
- [22] Daan Lenstra, B Verbeek, and A Den Boef. "Coherence collapse in single-mode semiconductor lasers due to optical feedback". In: *IEEE Journal of Quantum Electronics* 21.6 (1985), pp. 674–679.
- [23] Silvano Donati and Ray-Hua Horng. "The diagram of feedback regimes revisited". In: *IEEE Journal of selected topics in quantum electronics* 19.4 (2013), pp. 1500309–1500309.
- [24] Tin Komljenovic et al. "Widely tunable narrow-linewidth monolithically integrated external-cavity semiconductor lasers". In: *IEEE Journal of Selected Topics in Quantum Electronics* 21.6 (2015), pp. 214–222.
- [25] Amnon Yariv and Michiharu Nakamura. "Periodic structures for integrated optics". In: *IEEE Journal of Quantum Electronics* 13.4 (1977), pp. 233–253.
- [26] Uwe Feiste. "Optimization of modulation bandwidth in DBR lasers with detuned Bragg reflectors". In: *IEEE journal of quantum electronics* 34.12 (1998), pp. 2371–2379.
- [27] Olle Kjebon et al. "Two-section InGaAsP DBR-lasers at 1.55/spl mu/m wavelength with 31 GHz direct modulation bandwidth". In: *Indium Phosphide and Related Materials, 1997., International Conference on*. IEEE. 1997, pp. 665–668.

-
- [28] Marek Chacinski and Richard Schatz. “Impact of losses in the Bragg section on the dynamics of detuned loaded DBR lasers”. In: *IEEE Journal of Quantum Electronics* 46.9 (2010), pp. 1360–1367.
 - [29] Asier Villafranca, Javier Lasobras, and Ignacio Garcés. “Precise characterization of the frequency chirp in directly modulated DFB lasers”. In: *Electron Devices, 2007 Spanish Conference on*. IEEE. 2007, pp. 173–176.
 - [30] Christoph Harder, Kerry Vahala, and Amnon Yariv. “Measurement of the linewidth enhancement factor α of semiconductor lasers”. In: *Applied Physics Letters* 42.4 (1983), pp. 328–330.
 - [31] Marco Vallone, Paolo Bardella, and Ivo Montrosset. “Enhanced modulation bandwidth in complex cavity injection grating lasers”. In: *IEEE Journal of Quantum Electronics* 47.10 (2011), pp. 1269–1276.
 - [32] Kerry Vahala and Amnon Yariv. “Detuned loading in coupled cavity semiconductor lasers—effect on quantum noise and dynamics”. In: *Applied Physics Letters* 45.5 (1984), pp. 501–503.
 - [33] GOVIND P Agrawal and CHARLES H Henry. “Modulation performance of a semiconductor laser coupled to an external high-Q resonator”. In: *IEEE journal of quantum electronics* 24.2 (1988), pp. 134–142.
 - [34] Kerry Vahala, Joel Paslaski, and Amnon Yariv. “Observation of modulation speed enhancement, frequency modulation suppression, and phase noise reduction by detuned loading in a coupled-cavity semiconductor laser”. In: *Applied Physics Letters* 46.11 (1985), pp. 1025–1027.
 - [35] Ivo Montrosset and Paolo Bardella. “Laser dynamics providing enhanced-modulation bandwidth”. In: *Semiconductor Lasers and Laser Dynamics VI*. Vol. 9134. International Society for Optics and Photonics. 2014, 91340H.
 - [36] JP Reithmaier et al. “Modulation speed enhancement by coupling to higher order resonances: a road towards 40 GHz bandwidth lasers on InP”. In: *Indium Phosphide and Related Materials, 2005. International Conference on*. IEEE. 2005, pp. 118–123.
 - [37] Moustafa Ahmed et al. “Enhancing modulation bandwidth of semiconductor lasers beyond 50 GHz by strong optical feedback for use in millimeter-wave radio over fiber links”. In: *Japanese Journal of Applied Physics* 52.12R (2013), p. 124103.
 - [38] Geert Morthier, Richard Schatz, and Olle Kjebon. “Extended modulation bandwidth of DBR and external cavity lasers by utilizing a cavity resonance for equalization”. In: *IEEE Journal of Quantum Electronics* 36.12 (2000), pp. 1468–1475.
 - [39] C Bornholdt et al. “40 Gbit/s directly modulated passive feedback DFB laser for transmission over 320 km single mode fibre”. In: *Optical Communication, 2008. ECOC 2008. 34th European Conference on*. IEEE. 2008, pp. 1–2.
 - [40] RF Broom. “Self modulation at gigahertz frequencies of a diode laser coupled to an external cavity”. In: *Electronics Letters* 23.5 (1969), pp. 571–572.
 - [41] R Broom et al. “Microwave self-modulation of a diode laser coupled to an external cavity”. In: *IEEE Journal of Quantum Electronics* 6.6 (1970), pp. 328–334.

Bibliography

- [42] Alexei A Tager and Klaus Petermann. “High-frequency oscillations and self-mode locking in short external-cavity laser diodes”. In: *IEEE Journal of Quantum Electronics* 30.7 (1994), pp. 1553–1561.
- [43] Stefan Bauer et al. “Nonlinear dynamics of semiconductor lasers with active optical feedback”. In: *Physical Review E* 69.1 (2004), p. 016206.
- [44] Rodney Tucker. “High-speed modulation of semiconductor lasers”. In: *Journal of Lightwave Technology* 3.6 (1985), pp. 1180–1192.
- [45] Govind P Agrawal and Niloy K Dutta. *Semiconductor lasers*. Springer Science & Business Media, 2013.
- [46] F Devaux, Y Sorel, and JF Kerdiles. “Simple measurement of fiber dispersion and of chirp parameter of intensity modulated light emitter”. In: *Journal of Lightwave Technology* 11.12 (1993), pp. 1937–1940.
- [47] RC Srinivasan and JC Cartledge. “On using fiber transfer functions to characterize laser chirp and fiber dispersion”. In: *IEEE Photonics Technology Letters* 7.11 (1995), pp. 1327–1329.
- [48] Leif Bjerkan et al. “Measurement of laser parameters for simulation of high-speed fiberoptic systems”. In: *Journal of Lightwave Technology* 14.5 (1996), pp. 839–850.

A. Appendix

A.1. Detuned Loading Condition Calculation

```
...  
Created on Sep 9, 2018  
@author: tqian  
  
import scipy  
import numpy as np  
from numpy import pi  
import matplotlib.pyplot as plt  
plt.style.use('classic')  
plt.rcParams.update(  
    {'font.family': 'Arial', 'font.size': 15, 'axes.linewidth': 2, 'xtick.major.width': 2, 'ytick.major.width': 2})  
from matplotlib.ticker import FormatStrFormatter  
  
c = 3e8  
n_gain = 3.2  
n_air = 1.  
n_poly = 1.46  
WL = np.linspace(1548e-9, 1552e-9, 10000)  
WL_D = 1550e-9  
freq = c / WL  
freq_center = c / (WL_D)  
L_gain = 300e-6  
L_phase = 525 * 1e-6  
L_grat = 700.644e-6  
L_grat_eff = L_grat/2  
L_poly = L_phase + L_grat_eff  
  
L_ext = (267 + 518.362787842 + 688) * 1e-6  
r_1 = 0.99  
r_ext = 0  
  
kappa_L = 0.68641  
kappa = kappa_L / L_grat  
print(kappa)  
  
delta_beta = 2 * pi * n_poly * (1 / WL - 1 / WL_D)  
gama = np.sqrt(kappa**2 + (1j * delta_beta)**2)  
r = 1j * kappa * np.sinh(gama * L_grat) / ((1j * delta_beta) *  
                                         np.sinh(gama * L_grat) + gama * np.cosh(gama * L_grat))  
r_bragg = np.abs(r)  
r_phi = (np.angle(r)) / pi  
  
W1 = np.exp(-2j * (2 * pi * n_poly * L_phase / WL))  
W2 = np.exp(-2j * (2 * pi * n_poly * L_ext / WL))  
r_eff = (r + r_ext * W2) / (1 + r * r_ext * W2) * W1  
  
gain = 22 * 100      # 27.368 cm^-1  
  
beta_3 = 2 * pi * n_gain / WL + 1j * (gain) / 2  
G = r_1 * np.exp(-2j * (beta_3 * L_gain)) * r_eff  
r_bragg = np.abs(r)  
r_phi = (np.angle(r)) / pi  
G_abs = np.abs(G)  
G_phi = np.angle(G) / (pi)  
  
fig, ax1 = plt.subplots()  
color = 'blue'  
ax1.set_xlabel('Detuned Frequency [GHz]', fontsize=20)  
  
ax1.set_ylabel('Round Trip Gain $|G|$', fontsize=20)  
x_axis = ((freq - freq_center) / 1e9)  
y_axis = G_abs ** 2  
ax1.plot(x_axis, y_axis, label="$R_{\{grating\}}$*", color='black')  
ax1.tick_params(axis='both', which='both', top=False, right=False)
```

A. Appendix

```
ax1.plot(x_axis[6000], y_axis[6000], '#F14040', marker='o', markersize=10)
ax1.plot(x_axis[4000], y_axis[4000], '#515151', marker='o', markersize=10)
ax1.axvline(x=x_axis[6000], color='#F14040', linestyle='--')
ax1.axvline(x=x_axis[4000], color='#515151', linestyle='--')
fig.tight_layout()

plt.show()
```

A.2. Photon-Photon Resonance Calculation

```
...
Created on Sep 12, 2018

@author: tqian

import scipy
import numpy as np
from numpy import pi
import cmath
import math
import matplotlib.pyplot as plt
from matplotlib.ticker import FormatStrFormatter

c = 3e8
WL = np.linspace(1548e-9, 1552e-9, 10000)
WL_D = 1550e-9
freq = c / WL
freq_center = c / (WL_D)
L_A = 140e-6
L_G = 780e-6
L_P = 0e-6

r1 = np.sqrt(0.99)
r1 = 0.32
r_ext = np.sqrt(0.1)

r_ext = 0
n_gain = 3.7
n_air = 1.
n_poly = 1.46
n_poly = 3.2
n_clad = 1.45
n_core = 1.48
n_eff = 3.244
n_eff = 3.7

kappa = 20 * 100
kappa_L = kappa * L_G

delta_f_z = c / (n_gain * L_G * np.sqrt(1 + (kappa_L / pi)**2))
print("delta_f_z=%sGHz" % (delta_f_z / 1e9))

delta_f_A = c / (2 * (n_gain * L_A + n_gain * L_G))
print("delta_f_A=%sGHz" % (delta_f_A / 1e9))

delta_f_T = c / (2 * (n_gain * L_A + n_eff * (L_G)))
print("delta_f_T=%sGHz" % (delta_f_T / 1e9))

R_BGA = delta_f_z / delta_f_A
print("R_BGA=%s" % (R_BGA))

delta_beta = 2 * pi * n_eff * (1 / WL - 1 / WL_D)
delta = delta_beta
gama = np.sqrt(kappa**2 + (1j * delta_beta)**2)

T11 = np.cosh(gama * L_G) - 1j * delta / gama * np.sinh(gama * L_G)
T12 = -1j * kappa / gama * np.sinh(gama * L_G)
T21 = 1j * kappa / gama * np.sinh(gama * L_G)
T22 = np.cosh(gama * L_G) + 1j * delta / gama * np.sinh(gama * L_G)
det_T = T11 * T22 - T21 * T12

r = 1j * kappa * np.sinh(gama * L_G) / (((1j * delta_beta) *
np.sinh(gama * L_G) + gama * np.cosh(gama * L_G)))

beta_1 = 2 * pi * n_poly / WL
beta_2 = 2 * pi * n_poly / WL
W1 = np.exp(-2j * (beta_1 * L_G))
W2 = np.exp(-2j * (beta_2 * L_P))      # without propagation loss

gain = 27.368 * 100      # 27.368 cm^-1
gain = 16 * 100
```

```

gain = 100 * 100
beta_3 = 2 * pi * n_gain / WL + 1j * (gain / 2)
G = r1 * np.exp(-2j * (beta_3 * L_A)) * r

r_bragg = np.absolute(r)
r_phi = (np.angle(r)) / pi

r_eff_ref = np.absolute(r_eff)
r_eff_phi = np.angle(r_eff) / pi

G_abs = np.absolute(G)
G_phi = np.angle(G) / pi

# 1st plot
fig, ax1 = plt.subplots()
color = 'blue'
ax1.set_xlabel('Frequency (GHz)')
ax1.set_ylabel('Reflectivity $R_{bragg}$', color=color)
ax1.plot(((freq - freq_center) / 1e9), r_bragg **
          2, label="$R_{bragg}$", color=color)
ax1.tick_params(axis='y', labelcolor=color)
ax1.grid()

ax2 = ax1.twinx() # instantiate a second axes that shares the same x-axis
color = 'green'
ax2.set_ylabel('Phase/$\pi$', color=color)
ax2.plot(((freq - freq_center) / 1e9), (r_phi),
          label="$\phi_{bragg}$", color=color)
ax2.tick_params(axis='y', labelcolor=color)
ax2.xaxis.set_major_formatter(FormatStrFormatter('.1f'))
plt.title("$r_{ext}=%s, L_{ext}=%s_mm" % (r_ext, L_P * 1000))
fig.tight_layout() # otherwise the right y-label is slightly clipped

# 2nd plot
(freq - freq_center)
fig, ax1 = plt.subplots()
color = 'blue'
ax1.set_xlabel('Frequency (GHz)')
ax1.set_ylabel('Round-Trip Gain $|G|$', color=color)
ax1.plot(((freq - freq_center) / 1e9), (G_abs**2), label="$|G|$", color=color)
ax1.set_xlim(-100, 100)
ax1.tick_params(axis='y', labelcolor=color)
ax1.grid()

ax2 = ax1.twinx() # instantiate a second axes that shares the same x-axis
color = 'green'
ax2.set_ylabel('Phase/$\pi$', color=color)
ax2.plot(((freq - freq_center) / 1e9), (G_phi), label="$\phi$", color=color)
ax2.set_xlim(-100, 100)
ax2.tick_params(axis='y', labelcolor=color)
ax2.xaxis.set_major_formatter(FormatStrFormatter('.1f'))
plt.title("$r_{ext}=%s, L_{ext}=%s_mm" % (r_ext, L_P * 1000))
fig.tight_layout() # otherwise the right y-label is slightly clipped

plt.show()

```